Ana Catarina Serra Tomás

Licenciada em Biologia Celular e Molecular

Targeted inhibition of *PIK3CA* mutations in glioma cell models

Dissertação para obtenção do Grau de Mestre em
Genética Molecular e Biomedicina

Orientadora: Doutora Marta Sofia Pojo Sousa, Investigadora Principal, Instituto Português de Oncologia de Lisboa Francisco Gentil

Co-orientadora: Prof. Doutora Margarida Casal Ribeiro Castro Caldas Braga, Professora Auxiliar, Faculdade de Ciências e Tecnologia, Universidade Nova de Lisboa

Júri

Presidente: Prof. Doutora Maria Alexandra Núncio de Carvalho Ramos Fernandes

Arguente: Doutor Filipe Manuel Teixeira Pinto

Vogal: Doutora Marta Sofia Pojo Sousa

FACULDADE DE CIÊNCIAS E TECNOLOGIA
UNIVERSIDADE NOVA DE LISBOA

Novembro, 2020

Ana Catarina Serra Tomás

Licenciada em Biologia Celular e Molecular

Targeted inhibition of *PIK3CA* mutations in glioma cell models

Dissertação para obtenção do Grau de Mestre em
Genética Molecular e Biomedicina

Orientadora: Doutora Marta Sofia Pojo Sousa, Investigadora Principal, Instituto Português de Oncologia de Lisboa Francisco Gentil

Co-orientadora: Prof. Doutora Margarida Casal Ribeiro Castro Caldas Braga, Professora Auxiliar, Faculdade de Ciências e Tecnologia, Universidade Nova de Lisboa

FACULDADE DE CIÊNCIAS E TECNOLOGIA
UNIVERSIDADE NOVA DE LISBOA

Novembro, 2020

Targeted inhibition of *PIK3CA* mutations in glioma cell models

Agradecimentos

Gostaria de agradecer a todos os que me acompanharam neste ano bastante desafiante e que contribuíram de alguma forma para a realização deste trabalho.

À minha orientadora, Doutora Marta Pojo, por me ter dado a oportunidade de trabalhar na sua equipa, o que me proporcionou uma experiência incrível e me permitiu aprender imenso, especialmente sobre o verdadeiro valor do trabalho em equipa e a importância da comunicação clara na ciência. Por sempre me apoiar e puxar por mim, para que pudesse dar o meu melhor, sempre. Pela excelente orientação, obrigada!

À minha co-orientadora, Professora Margarida Castro Caldas, pela disponibilidade demonstrada logo desde início e por todo o *feedback* valioso que me ofereceu.

A todos os membros do Grupo de Estudos do Melanoma. À Cheila Brito, a minha companheira de laboratório constante, por todos os ensinamentos e conhecimento que me transmitiu; por todo o apoio e encorajamento quando as coisas corriam menos bem; por todos os conselhos e boa disposição, que foram essenciais à minha aprendizagem e à-vontade no laboratório. À Mafalda Leite e à Sara Ventura, pelas críticas construtivas e discussões produtivas nas reuniões de laboratório. Ao José Maximino e Renato Ferreira, os mais recentes membros do grupo, pela animação que trazem todos os dias e pela vontade de ajudar. Ao Rafael Luís que, apesar de já não fazer parte do grupo, foi imprescindível no início desta etapa.

Aos grupos da Endocrinologia, Citogenética, e Metabolismo e Microambiente Tumoral da UIPM, por toda a ajuda e disponibilidade. Em especial, à Doutora Lúcia Roque pelo seu *expertise* em gliomas e toda a simpatia demonstrada, à Carolina Pires por me ter acompanhado na aventura dos Western blots e à Cindy Mendes pela ajuda na citometria de fluxo.

Às minhas grandes amigas: Andreia, Catarina, Inês, Jekinha e Nina, por estarem sempre presentes para me apoiar, mesmo que não seja presencialmente; por festejarem comigo as minhas conquistas e me confortarem nos momentos mais baixos.

Ao George, por toda a força que me transmite; por todas as noites em que cheguei a casa exausta e tive o jantar à minha espera; pela companhia durante a quarentena e o apoio durante as minhas crises existenciais.

Por fim, quero agradecer à minha família pelo apoio incondicional. Tudo o que tenho realizado só é possível graças a eles, que acreditam sempre e com convicção que sou capaz de ultrapassar qualquer obstáculo e concretizar os meus objetivos, mesmo quando eu duvido de mim mesma.

Abstract

Gliomas are the most common and lethal brain tumors in adults, with efficient therapies non-existent. *PIK3CA* mutations are potential therapeutic targets, described as early constitutive events in glioblastomas (GBM).

The goal of this project was to assess the impact of *PIK3CA* mutations on glioma aggressiveness and evaluate the inhibition of PI3Kα in glioma cell models harboring *PIK3CA* mutations. Additionally, we intended to characterize the IPOLFG cohort with *IDH2* mutational analysis, previously classified according to *IDH1* and *PIK3CA* mutational status and 1p19q co-deletion.

Thus, *IDH2* mutations were evaluated by Sanger sequencing, and immune cell infiltrates were estimated using the TIMER platform. Functional studies were performed using a GBM cell line – U87MG, transfected to contain E545K and H1047R mutations. The effects of temozolomide and alpelisib treatment on cell viability, death, and PI3K/AKT pathway activation were assessed.

Only one out of 279 sequenced samples harbored an *IDH2* mutation. *PIK3CA* mutation frequencies remained unaltered in glioma molecular subgroups.

Using TIMER analysis, we observed increased CD8+ T cell infiltration in *PIK3CA* mutant low-grade gliomas, whilst *PIK3CA* and *STAT5B* expressions were positively correlated.

Regarding *PIK3CA* mutations on glioma aggressiveness, no differences were observed in U87MG colony formation, migration, or invasion, regardless of *PIK3CA* mutational status. Moreover, *PIK3CA* mutations did not change U87MG cells' sensitivity to either alpelisib or temozolomide, with alpelisib potentiating PI3K/AKT signaling.

Here, we achieved a more refined characterization of the IPOLFG glioma cohort and uncovered a possible, novel link between tumor microenvironment and the prevalence of *PIK3CA* mutations during glioma progression. Our data shows that *PIK3CA* mutations neither significantly impact GBM cell aggressiveness nor confer added sensitivity to PI3Kα targeted inhibition. Nevertheless, we found that GBM cells seem to trigger complex, not yet described compensatory mechanisms, which could pave the way for future studies relating pan-PI3K inhibitors and the targeting of other pathways.

Keywords: gliomas; *PIK3CA*; *IDH2*; U87MG; alpelisib; temozolomide

Resumo

Gliomas são os tumores cerebrais mais comuns e letais em adultos, não existindo terapias eficientes. Mutações no gene *PIK3CA* são potenciais alvos terapêuticos, descritas como eventos precoces e constitutivos em glioblastomas (GBM).

Neste projeto pretendemos aferir o impacto das mutações em *PIK3CA* na agressividade dos gliomas e avaliar a inibição de PI3Kα em modelos celulares de glioma *PIK3CA* mutados. Adicionalmente, tencionámos caracterizar o *cohort* do IPOLFG com análise mutacional do gene *IDH2*, tendo sido previamente classificado de acordo com o estado mutacional de *IDH1* e *PIK3CA*, e a codeleção 1p/19q.

Assim, mutações em *IDH2* foram avaliadas por sequenciação de Sanger, e infiltrados de células do sistema imunitário estimados recorrendo a TIMER. Estudos funcionais foram efetuados utilizando uma linha celular de GBM – U87MG, transfetada para conter as mutações E545K e H1047R. O efeito da temozolamida e alpelisib na viabilidade e morte celular, e na via PI3K/AKT foi avaliado.

Apenas uma em 279 amostras sequenciadas apresentou mutação em *IDH2*. As frequências das mutações *PIK3CA* permaneceram inalteradas nos subgrupos moleculares de glioma.

Utilizando a análise por TIMER, observámos um aumento na infiltração de células T CD8+ em gliomas de baixo grau *PIK3CA* mutados, e as expressões de *PIK3CA* e *STAT5B* mostraram-se correlacionadas.

Relativamente às mutações *PIK3CA* na agressividade de gliomas, não se observaram diferenças na formação de colónias, migração ou invasão de células U87MG, independentemente do estado mutacional de *PIK3CA*. Mutações neste gene também não alteraram a sensibilidade das células U87MG ao alpelisib ou temozolamida, sendo que alpelisib potenciou a via PI3K/AKT.

Aqui, conseguimos uma caracterização mais refinada do cohort de gliomas do IPOLFG e desvendámos uma nova possível ligação entre o microambiente tumoral e a prevalência das mutações *PIK3CA* durante a progressão dos gliomas. Os nossos dados indicam que as mutações *PIK3CA* não têm um impacto significativo na agressividade de células de GBM, nem conferem sensibilidade adicional à inibição seletiva de PI3Kα. Ainda assim, concluímos que as células de GBM parecem despoletar mecanismos de compensação complexos, ainda não descritos, o que poderá abrir portas para estudos futuros que relacionem inibidores pan-PI3K com a inibição de outras vias.

Termos-chave: gliomas; *PIK3CA*; *IDH2*; U87MG; alpelisib; temozolamida

Table of contents

List of figures

List of tables

List of abbreviations, symbols, and conventions

2-HG	D-2-hydroxyglutarate
AKT	Protein Kinase B
ALT	Alternative lengthening of telomeres
ANOVA	Analysis of variance
ATCC	American Type Culture Collection
ATP	Adenosine triphosphate
ATRX	Alpha Thalassemia/Mental Retardation Syndrome X-linked
Bcl-XL	B-cell lymphoma-extra large
BSA	Bovine serum albumin
BYL719	Phosphatidylinositol-4,5-biphosphate 3-kinase catalytic subunit alpha inhibitor, alpelisib
CCK8	Cell Counting Kit-8
CD	Cluster of differentiation
cDNA	Complementary deoxyribonucleic acid
CNS	Central Nervous System
DAPI	4'-6-diamidino-2-phenylindole
DMEM	Dulbecco's modified Eagle's medium
DMSO	Dimethyl sulfoxide
DNA	Deoxyribonucleic acid
ECM	Extracellular matrix
EDTA	Ethylenediaminetetraacetic acid
EGF	Epidermal growth factor
EGFR	Epidermal growth factor receptor
EGFRvIII	Epidermal growth factor receptor variant III
ER	Estrogen receptor
ERK	Extracellular signal-regulated kinase
FBS	Fetal bovine serum
g	Relative centrifugal force, g force
GBM	Glioblastoma multiforme
G-CIMP	Glioma CpG island methylator phenotype
HEPES	4-(2-hydroxyethyl)-1-piperazineethanesulfonic acid
HER2	Human epidermal growth factor receptor-2
IC_{50}	Half-maximal inhibitory concentration
IDH	Isocitrate dehydrogenase
iNHA	Immortalized normal human astrocytes
IPOLFG	Instituto Português de Oncologia de Lisboa Francisco Gentil
LGG	Low-grade gliomas
MAPK	Mitogen-activated protein kinase

MGMT	O-6-methylguanine-DNA methyltransferase
MITC	3-methyl-(triazene-1-yl)imidazole-4-carboxamide
MMP	Matrix metalloproteinase
mRNA	Messenger ribonucleic acid
mTOR	Mechanistic target of rapamycin
mTORC1	Mechanistic target of rapamycin complex 1
NADP+	Nicotinamide adenine dinucleotide phosphate
NK	Natural Killer
p	*p*-value
P/S	Penicillin/streptomycin
p110	Phosphatidylinositol-4,5-biphosphate 3-kinase catalytic subunit
p85	Phosphatidylinositol-4,5-biphosphate 3-kinase regulatory subunit
PBS	Phosphate-buffered saline
PCR	Polymerase chain reaction
PCV	Procarbazine/lomustine/vincristine
PDK	Phosphatidylinositol-dependent kinases
PET	Polyethylene terephthalate
PI	Propidium iodide
PI3K	Phosphatidylinositol-4,5-bisphosphate 3-kinase
PIK3CA	Phosphatidylinositol-4,5-biphosphate 3-kinase catalytic subunit alpha
PIK3CB	Phosphatidylinositol-4,5-biphosphate 3-kinase catalytic subunit beta
PIK3CD	Phosphatidylinositol-4,5-biphosphate 3-kinase catalytic subunit delta
PIK3CG	Phosphatidylinositol-4,5-biphosphate 3-kinase catalytic subunit gamma
PIP_2	Phosphatidylinositol-4,5-bisphosphate
PIP_3	Phosphatidylinositol-3,4,5-trisphosphate
PTEN	Phosphatase and Tensin Homologue
PVDF	Polyvinylidene difluoride
RIPA	Radioimmunoprecipitation assay
RNA	Ribonucleic acid
rpm	Revolutions per minute
RT-qPCR	Reverse transcriptase quantitative polymerase chain reaction
SDS	Sodium dodecyl sulfate
SEM	Standard error of the mean
STAT5B	Signal transducer and activator of transcription 5B
TAM	Tumor-associated macrophages
TBE	Tris/Borate/Ethylenediaminetetraacetic acid
TCA	Tricarboxylic acid
TCGA	The Cancer Genome Atlas
TERT	Telomerase Reverse Transcriptase

TET	Ten-eleven translocation
TIMER	Tumor Immune Estimation Resource
TME	Tumor microenvironment
TMZ	Temozolomide
Tregs	Regulatory T cells
TSC2	Tuberculosis sclerosis complex 2
U87MG	Glioblastoma cell line
WHO	World Health Organization
WT	Wildtype
α-KG	α-ketoglutarate

1. Introduction

1.1. Hallmarks of Cancer

Cancer can be defined as a group of diseases associated with abnormal cell growth caused by the transformation of normal cells to malignant cells[1]. Accumulative changes in the genome and gene expression lead to the dysregulation of multiple signaling pathways, allowing malignant cells to rapidly proliferate, invade surrounding tissue and metastasize to distant sites, which can ultimately lead to death[2]. Cancer is, therefore, one of the leading causes of death in developed countries, responsible for an estimated 18.1 million new cases and 9.6 million deaths in 2018 worldwide[3]. With the population rapidly growing, aging, and adopting increasingly unhealthy lifestyles, cancer incidence and mortality are expected to rise internationally[3]. Advances in cancer prevention, diagnostics and therapeutics are thus imperative to its early detection and elimination.

The discovery of oncogenes and tumor suppressor genes was one of the first steps to better understand this heterogenous, multidimensional and dynamic disease[4,5]. An oncogene arises from the activation of a proto-oncogene, whether through gene amplification or activating mutations. Since proto-oncogenes include genes related to the positive regulation of the cell cycle, they promote cell proliferation and survival when upregulated, thus contributing to tumorigenesis[4]. On the other hand, tumor suppressor genes are linked to the negative regulation of the cell cycle and are consequently usually impaired in cancer through inactivating mutations[5].

However, these genetic alterations are not enough to fully explain the complexity of cancer. In 2000, Hanahan and Weinberg shed light on the multistep process of human tumorigenesis by describing six hallmarks of cancer – traits shared by most human cancers that allow malignant cells to survive, proliferate and disseminate[6]. Self-sufficiency in growth signals, insensitivity to anti-growth signals, evasion of apoptosis, limitless replicative potential, sustained angiogenesis, and tissue invasion and metastasis were the six hallmarks proposed, defined as acquired functional capabilities[6]. Additionally, genome instability was considered an enabling characteristic of cancer, necessary for acquiring the mentioned hallmarks[6].

Eleven years later, the same authors proposed two new emerging hallmarks of cancer, as well as a new enabling characteristic[7]. Reprogramming energy metabolism was one of the suggested hallmarks, since tumor cells favor glycolysis rather than oxidative phosphorylation, even in the presence of oxygen, an observation designated as the Warburg effect[7]. With the growing understanding of the pivotal role the tumor microenvironment plays in cancer progression, evading immune destruction was also classified as an emerging hallmark[7]. Furthermore, tumor-promoting inflammation was described as contributing to the acquisition of the core hallmarks of cancer through the release of several bioactive molecules and mutagenic chemicals[7].

It is now generally accepted that cancer development is comparable to Darwinian evolution; both genome instability and tumor-promoting inflammation enable cells to acquire a series of functional capabilities – the hallmarks of cancer discussed previously, depicted in **Figure 1.1** –, regarded as selective advantages that aid in the transformation of normal cells to tumor cells[6,7]. Hence, inhibition of these cancer hallmarks should, theoretically, arrest tumor growth and development, assisting in its

eradication. So far, targeted therapies toward one or a few cancer hallmarks have not been very successful[7]. However, therapies targeting multiple hallmarks simultaneously could prove to be more effective[7,8].

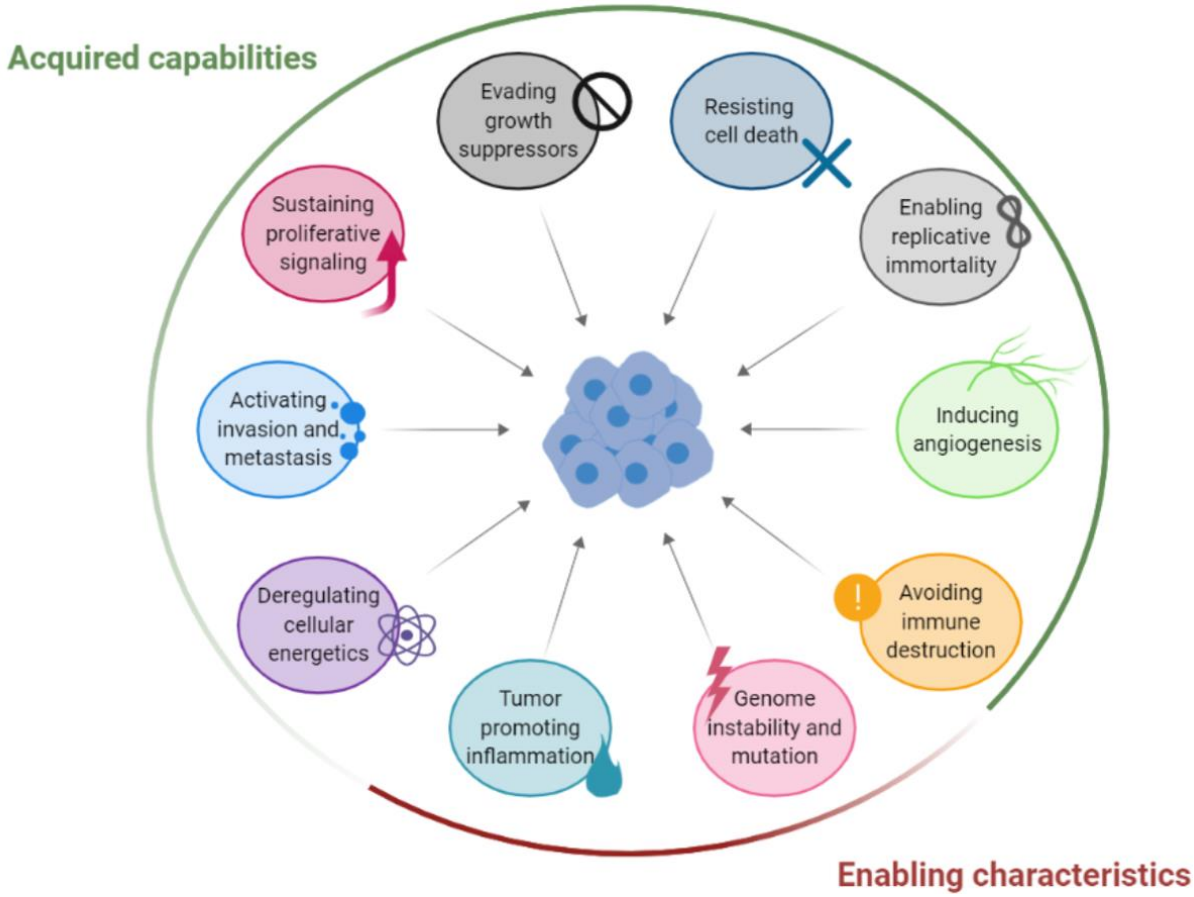

Figure 1.1. The Hallmarks of Cancer. The eight acquired functional capabilities (green) as well as both enabling characteristics (red) proposed by Hanahan and Weinberg[6,7] are represented. These hallmarks of cancer can be exploited as targets in the development of therapeutic strategies against cancer. Adapted[7].

Even though the hallmarks of cancer are now viewed as key players in cancer development and evolution, Hanahan and Weinberg's work received some criticism. Some studies propose other characteristics as hallmarks of cancer, such as loss of differentiation[8] and aberrant glycosylation[9]. It is also important to acknowledge that the hallmarks of cancer are co-dependent and complement each other, and not all hallmarks are continually displayed by all cells in a tumor[8,10]. Knowing that tumors are heterogenous and multidimensional entities, always evolving, it makes sense that the cancer hallmarks behave in a similar, dynamic way.

1.2. Central Nervous System Tumors

Tumors of the central nervous system (CNS) can affect both children and adults in very distinct ways[11], with the brain being the most common site for these neoplasms (>90%) and the remainder occurring in the spinal cord, meninges and cranial nerves[12]. The CNS tumor spectrum embraces

gliomas, ependymomas, choroid plexus tumors, medulloblastomas, meningiomas, neuronal and mixed neuronal-glial tumors, varying widely in location, histology, grade and prognosis[13].

In children, brain tumors are the most common solid malignancy and have a profound negative impact on the developing CNS[14]. However, pediatric CNS tumors are vastly different entities from adult CNS tumors and are thus studied separately[11]. In this work, we will focus on adult CNS tumors.

Overall, adult CNS tumors are relatively infrequent. In 2016, there were only an estimated 330 000 incident cases of these tumors worldwide[12], and malignant primary brain tumors are thought to represent only 1.4% of all cancers in adults[15]. Consequently, less resources are allocated and prioritized for the management of these diseases[12]. However, adult cancer of the CNS is associated with high mortality rates and poor prognosis, being responsible for 227 000 deaths globally, in 2016[12]. Additionally, it is also associated with cognitive impairment, loss of independent functioning, and profound and disabling effects on general health and quality of life[12,15].

The therapies most often administered to CNS tumor patients involve surgical resection, radiotherapy and/or chemotherapy[15]. Some studies suggest that, in cases where it is viable, surgical resection has been associated with better outcomes and quality of life[15–17]. Conversely, long-term cognitive changes can be detected after widespread radiation and chemotherapy[15,18].

Hardly any risk factors are known to be implicated in CNS tumors. Some genetic syndromes are related to a higher risk of developing CNS cancer, but their overall frequency is very low[19]. Furthermore, positive associations with ionizing radiation have been found, making it the only accepted environmental risk factor correlated with these tumors, as well as negative associations with atopic conditions[12]. As such, not many strategies can be employed to prevent the appearance of these neoplasms, highlighting the need for early diagnosis and effective therapies.

1.3. Gliomas

Despite representing only 27% of all primary CNS tumors, gliomas are the most common malignant primary brain tumors in adults (~80%)[20]. Although these neoplasms appear most frequently in the brain, they can also occur in the brain stem, cerebellum and spinal cord[21]. These tumors are highly heterogenous and invasive, frequently infiltrating surrounding tissues without metastasizing to other organs[22,23]. Therapeutic strategies usually consist of maximal surgical resection, followed by radiotherapy and chemotherapy. However, complete resection is impossible and these strategies often fail due to glioma cell invasion, ultimately leading to tumor recurrence[22,23]. Consequently, gliomas hold dismal prognosis and are considered the neoplasms associated with the highest number of years of potential life lost[23].

Gliomas result from the malignant transformation of glial cells, such as astrocytes, oligodendrocytes and ependymal cells, or their precursors[23]. Normal glial cells comprise a large portion of the human brain and support neuronal function, retaining their proliferative ability during adulthood, as opposed to most neurons[24]. Together, these characteristics might contribute to the higher incidence of gliomas when compared with other CNS malignancies[20].

Until recently, gliomas were classified based exclusively on histological criteria, according to morphological similarities between tumor cells and glial cells, giving rise to three main histological types – oligodendroglial, astrocytic and oligoastrocytic tumors[25]. Furthermore, these tumors were graded on a malignancy scale, from I to IV – grade I was associated with a better prognosis and lower anaplasia, whilst grade IV applied to mitotically active neoplasms with the highest degree of anaplasia, often fatal[25].

Oligodendroglial tumors were comprised of oligodendrogliomas (grade II) and anaplastic oligodendrogliomas (grade III)[25]. These entities derive from oligodendrocytes (or their precursors), which are responsible for myelin production in the CNS, imperative to the proper conduction of the electric impulse through the neuronal axons[24,25].

On the other hand, astrocytic tumors derive from astrocytes (or their precursors), which perform a multitude of important functions in the CNS, including maintenance of the blood-brain barrier, ion homeostasis, integration in tripartite synapses through the transport of neurotransmitters, metabolic and structural support to neurons, and neuroprotection[24–26]. Astrocytic tumors include different subtypes of astrocytomas, ranging from grade I to grade IV. Grade IV astrocytomas are most commonly designated as glioblastomas (GBM, glioblastoma multiforme), which represent the most aggressive and lethal subtype of glioma[23,25]. GBM is the most prevalent tumor among gliomas, with a median patient survival of about 12 months[23].

Lastly, oligoastrocytic tumors, or mixed gliomas, included oligoastrocytomas (grade II) and anaplastic oligoastrocytomas (grade III), and presented morphological similarities with both oligodendrocytes and astrocytes[20,25].

However, the histological classification of gliomas had several limitations. It was associated with high intra- and interobserver variability, especially pertaining to grade II and grade III gliomas[27]. Additionally, there was also high heterogeneity among histological subgroups. The glioblastoma subtype, for example, contained distinct tumor groups that differed regarding prognosis, age of onset, location and clinical outcome[23]. Moreover, some subtypes, such as oligoastrocytoma, were not clearly defined entities nor were they associated with any molecular profile[23]. All of these uncertainties made it quite challenging to accurately diagnose patients and predict clinical outcomes[23,27].

1.4. Glioma molecular stratification

Over the last decades there have been remarkable advances in molecular techniques, resulting in an increase of the knowledge about glioma molecular alterations[20]. As a result, the 2016 World Health Organization (WHO) classification of CNS tumors included isocitrate dehydrogenase (*IDH*) gene mutations and the 1p/19q codeletion as indispensable molecular biomarkers for the stratification of gliomas[13]. Thus, this classification took a multilayered approach that combined molecular criteria, histological features and histological grade[23].

Gliomas are currently grouped into five main molecular subgroups – GBM *IDH*-wildtype, GBM *IDH*-mutant, astrocytoma *IDH*-wildtype, astrocytoma *IDH*-mutant, and oligodendroglioma *IDH*-mutant and 1p/19q-codeleted[13] (**Figure 1.2**). The diagnosis of oligoastrocytoma disappeared, since most

entities defined previously as oligoastrocytomas can now be classified as either astrocytoma or oligodendroglioma after genetic testing[13].

Approximately 90% of GBM cases are classified as *IDH*-wildtype, most common in patients over 55 years of age, and usually manifest as primary or *de novo* gliomas, characterized by the absence of pre-existing lower-grade neoplasms[13]. The remainder 10% of GBM cases are classified as *IDH*-mutant, mostly affecting younger patients and including secondary GBM developed from prior lower-grade diffuse gliomas[23]. Most importantly, patients with GBM *IDH*-mutant are more likely to have a better clinical outcome (median overall survival of 25 months) than GBM *IDH*-wildtype patients (median overall survival of 10 months), since *IDH* mutations are linked to better prognosis, longer survival and sensitivity to chemotherapy[23,28,29].

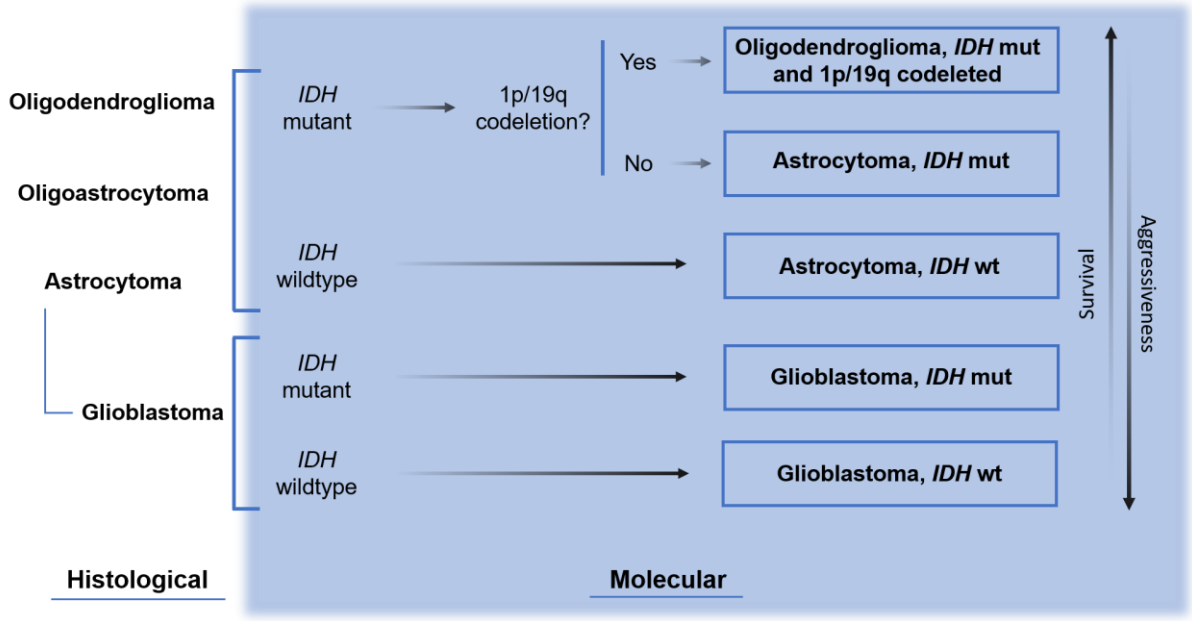

Figure 1.2. The histological and molecular classifications of gliomas. A simplified schematic representation that illustrates how gliomas are currently classified, based on both molecular and histological criteria. It is also possible to understand the differences between the previous unidimensional classification based solely on histological features and the current one, that is multilayered and considers both molecular biomarkers and histological characteristics. *IDH*, isocitrate dehydrogenase; mut, mutant; wt, wildtype.

Regarding astrocytomas, *IDH* mutations are also correlated with better prognosis. In fact, patients with astrocytoma *IDH*-wildtype generally have a prognosis more comparable to GBM than to astrocytoma *IDH*-mutant (median overall survival of 14 and 114 months, respectively)[20,29]. Contrarily to GBM, astrocytoma *IDH*-wildtype and astrocytoma *IDH*-mutant usually occur at similar frequencies[29].

Lastly, oligodendrogliomas are defined by whole-arm 1p/19q codeletion, due to the unbalanced t(1;19)(q10;p10) translocation, combined with *IDH* mutation[13,29]. In addition to *IDH* mutations being associated with better patient outcome, 1p/19q loss is also a good biomarker that indicates better prognosis[30]. Therefore, oligodendrogliomas are usually associated with the best prognosis out of all glioma subgroups, with a median overall survival of 198 months[13,29].

1.4.1. Glioma therapies

Gliomas are considered virtually incurable, with current therapies being non-efficient[23]. Standard therapy for both GBM *IDH*-wildtype and GBM *IDH*-mutant is known as the Stupp protocol and it involves maximal surgical resection followed by radiotherapy with concomitant and adjuvant temozolomide (TMZ)[31]. TMZ is an alkylating agent capable of crossing the blood-brain barrier, arresting the cell cycle and triggering apoptosis in tumor cells[20]. At physiological pH, TMZ spontaneously converts into 3-methyl-(triazene-1-yl)imidazole-4-carboxamide (MITC), a compound able to transfer a methyl group to DNA[32]. Among the adducts created, O-6-methylguanine seems to play a crucial role in the cytotoxicity of TMZ, introducing unrepairable mispairs with thymine in the DNA of glioma cells. As a result, single- and double-strand breaks are formed, culminating in cell apoptosis[23,32].

The median survival benefit obtained with the Stupp protocol is of 2.5 months[31]. Even though it represents an improvement in clinical outcome, prognosis remains extremely poor. Besides, partly due to high heterogeneity and infiltrative capability, GBM is known to resist administered therapies[22]. Thus, the need for new, more efficient therapeutic strategies is still vital.

Similarly to GBM, treatment of both astrocytoma molecular subgroups commonly involves surgical resection, if it can be safely performed, as gross total resection has been linked with better clinical outcomes, especially in patients with astrocytoma *IDH*-mutant[33]. After surgery, a combination of radiotherapy and TMZ can be administered to patients with astrocytoma *IDH*-mutant[34]. Furthermore, patients with astrocytoma *IDH*-wildtype that behaves similarly to GBM, presenting with an aggressive phenotype, often go through the Stupp protocol[34,35].

In oligodendroglioma, therapy also usually involves surgical resection when feasible[34]. Postoperative treatment includes radiotherapy followed by chemotherapy, since 1p/19q loss is associated with better chemotherapy response and better outcomes when chemotherapy is added to radiotherapy[27,34,35]. Particularly, patients benefit from adjuvant chemotherapy with procarbazine/lomustine/vincristine (PCV)[36] or TMZ[37].

1.5. Current and new potential molecular biomarkers in gliomas

1.5.1. *IDH* mutations

IDH is an enzyme involved in the tricarboxylic acid (TCA) cycle that catalyzes the conversion of isocitrate into α-ketoglutarate (α-KG), in a NADP+ dependent manner. This protein is encoded by *IDH1* in the cytoplasm and peroxisomes, and by *IDH2* in the mitochondria[28]. In gliomas, the main *IDH* mutation identified, representing roughly 90% of all *IDH* mutations, results in the conversion of an arginine residue at codon 132 of *IDH1* to a histidine residue (R132H). The remainder includes other substitutions at codon 132 of *IDH1* (R132C, R132L, R132S, R132G) and at codon 172 of *IDH2* (R172G, R172M, R172K), which are much rarer[20,38]. Both residues are located at the active site of the enzyme that binds to the substrate[38].

These mutations have shown to be early events in gliomagenesis that prevail during tumor progression. It is therefore hypothesized that they might be key players in glioma development[27]. However, *IDH* mutations are also related with better prognosis and patient outcome[23], as mentioned

previously. This happens because mutant IDH acquires a new function that results in the production of an oncometabolite, D-2-hydroxyglutarate (2-HG), from α-KG[23] (**Figure 1.3**). Hence, *IDH* mutations are always heterozygous; one wildtype allele is needed for the production of α-KG, that in turn serves as a substrate for the mutated enzyme, encoded by the mutant allele[28].

Structurally, α-KG and 2-HG are quite similar. As a result, 2-HG inhibits various α-KG-dependent dioxygenases, such as ten-eleven translocation (TET) 5-methylcytosine hydroxylases, which catalyze DNA demethylation through the conversion of 5-methylcytosine to 5-hydroxymethylcytosine[39]. Furthermore, 2-HG also inhibits the Jumonji-C-domain-containing histone-lysine demethylases[23]. Both DNA methylation and histone tail methylation are linked to gene expression regulation, by gene silencing and chromatin structure remodeling, respectively[40]. As such, *IDH* mutations lead to profound epigenetic changes through global hypermethylation of CpG islands and of histone tails, culminating in a glioma CpG island methylator phenotype (G-CIMP)[20] (**Figure 1.3**). This phenomenon could explain why *IDH* mutations ultimately promote gliomagenesis, since these alterations completely restructure the expression of multiple genes[28]. Additionally, 2-HG is also known to disturb collagen maturation, consequently weakening the basement membrane, and 2-HG mediated histone hypermethylation can block cancer cell differentiation[28]. One of the genes influenced by DNA hypermethylation is O-6-methylguanine-DNA methyltransferase (*MGMT*), with the promoter being significantly methylated in *IDH*-mutant gliomas[27,28].

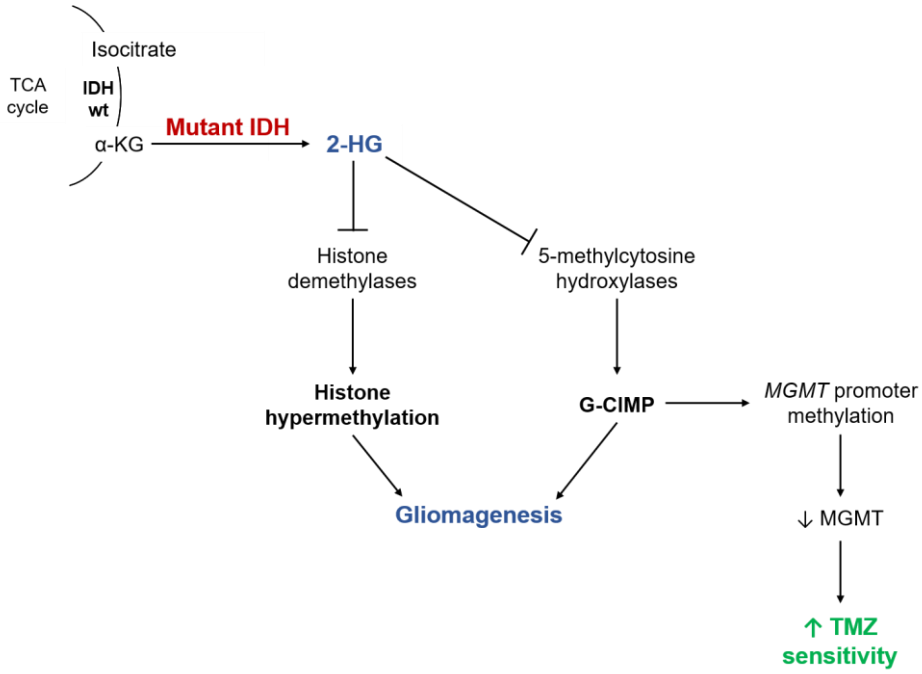

Figure 1.3. The contribution of *IDH* mutations to gliomagenesis and temozolomide sensitivity. Mutated IDH can convert α-KG to 2-HG, which in turn inhibits both histone and 5-methylcytosine demethylation. The result includes both histone hypermethylation and G-CIMP, contributing to gliomagenesis. Additionally, *MGMT* promoter methylation leads to reduced levels of MGMT and consequently increased TMZ sensitivity. Adapted[28]. IDH, isocitrate dehydrogenase; wt, wildtype; α-KG, α-ketoglutarate; 2-HG, 2-hydroxyglutarate; G-CIMP, glioma CpG Island methylator phenotype; MGMT, O-6-methylguanine-DNA methyltransferase; TMZ, temozolomide.

1.5.2. 1p/19q codeletion

The 1p/19q codeletion is one of the most important biomarkers currently used to molecularly stratify gliomas, together with *IDH* mutations. It arises due to the unbalanced t(1;19)(q10;p10) translocation[13]. It is an alteration typical of oligodendrogliomas and is considered a good biomarker that indicates better prognosis[30].

The addition of these molecular biomarkers to glioma classification has been related to a better and more precise segregation between different subgroups according to diagnosis, prognosis and response to therapy[29,41,42]. Still, there is much more room for improvement. Molecular subgroups remain quite heterogenous regarding clinical presentation and outcome as well as therapy resistance[27]. Particularly, GBM *IDH*-wildtype and astrocytoma *IDH*-wildtype include patients with a wide range of overall survival[29]. Additional molecular biomarkers are therefore needed to better understand these neoplasms, devise better therapeutic strategies and increase the accuracy of both glioma diagnosis and prognosis[27].

1.5.3. *MGMT* promoter methylation

MGMT is responsible for the repair of O-6-methylguanosine, by transferring the methyl group from the adduct to the enzyme itself, which in turn is marked for degradation[23]. Notably, O-6-methylguanosine is one of the adducts induced by TMZ treatment, as discussed previously. If MGMT expression levels are reduced due to *MGMT* promoter methylation, then the damages induced by TMZ will not be repaired. Therefore, *MGMT* promoter methylation is associated with higher TMZ sensitivity[23] (**Figure 1.3**). Contrarily, increased levels of *MGMT* mRNA resulting from the absence of promoter methylation are associated with the development of alkylating chemotherapy resistance[43]. It could then be hypothesized that *IDH* mutations are implicated in the sensitivity to chemotherapy and better prognosis through 2-HG production and consequent *MGMT* promoter methylation[27,43].

Interestingly, *MGMT* promoter methylation is itself described as a predictive biomarker of benefit from TMZ therapy[44]. Even though *MGMT* promoter methylation is most common in GBM patients with mutant *IDH*, our group showed that *MGMT* promoter methylation is associated with prolonged overall survival in GBM *IDH*-wildtype[29]. Furthermore, *MGMT* methylated gliomas were associated with a better response to chemo-radiotherapy, but not radiotherapy alone[29]. In these cases, *MGMT* methylation can be a helpful biomarker, guiding clinicians in the decision of the most appropriate and effective therapy[23]. Brito et al. even suggest the creation of a new molecular subgroup of *MGMT* methylated gliomas within GBM *IDH*-wildtype[29].

1.5.4. Alpha Thalassemia/Mental Retardation Syndrome X-linked gene (*ATRX*)

In recent years, several genes have been proposed as promising molecular biomarkers in a glioma context. One of these genes is related with the limitless replicative potential of tumor cells, a known hallmark of cancer – the Alpha Thalassemia/Mental Retardation Syndrome X-linked gene (*ATRX*)[23].

There are two fundamental mechanisms associated with telomere length maintenance, important in cell immortalization. One of them is designated Alternative Lengthening of Telomeres (ALT) and it

involves *ATRX*[45]. This gene is known to participate in chromatin remodeling and acts as an ALT repressor, regulating telomere length[23]. Thus, inactivating mutations in *ATRX* can promote tumorigenesis through ALT activation[45], and are present in approximately 70% of *IDH*-mutant astrocytomas[27]. These alterations also seem to be negatively correlated with the presence of the 1p/19q codeletion[20]. As a consequence, *ATRX* mutations have been recommended as biomarkers that aid in the distinction between astrocytomas *IDH*-mutant and oligodendrogliomas *IDH*-mutant and 1p/19q codeleted[13]. However, it was not included in the 2016 WHO glioma classification because it can also be found in some specific types of GBM *IDH*-wildtype[23].

1.5.5. Telomerase Reverse Transcriptase gene (*TERT*)

The enzyme telomerase is also linked to telomere length maintenance[45]. Hence, mutations in the promoter region of the telomerase reverse transcriptase gene (*TERT*) that ultimately activate telomerase are found in numerous cancer types[20]. In gliomas, these mutations are more prevalent in GBM *IDH*-wildtype (88%) and oligodendrogliomas *IDH*-mutant and 1p/19q codeleted (94%)[20,29]. While it might be pertinent to understand the role that these mutations play in gliomagenesis and tumor progression, the evaluation of *TERT* promoter mutational status does not seem to be advantageous to glioma classification, since it is present in a big majority of gliomas regardless of prognosis or clinical presentation[27,29].

1.5.6. Epidermal Growth Factor Receptor (*EGFR*)

Another important hallmark of cancer consists in self-sufficiency of growth signaling. Epidermal growth factor receptor (EGFR) is a tyrosine kinase capable of activating multiple signaling pathways involved in cell growth and survival[46]. *EGFR* amplifications arise in around 45% of GBM, with most also expressing a constitutively active variant (*EGFRvIII*)[20,27]. Considering the biological role of this kinase, it would be expected that activating molecular alterations would indicate worse clinical outcomes[43]. However, the use of this biomarker as a prognostic factor is controversial and routine evaluation of *EGFR* alterations does not seem very useful in gliomas[27,43]. In fact, these alterations seem to be more relevant when therapeutic strategies are mentioned. Recent evidences suggest that GBM *IDH*-wildtype patients with *EGFR* amplifications respond better to radiotherapy, through unknown mechanisms[29]. Moreover, *EGFR* targeted therapies could be promising, but have been unsuccessful in gliomas thus far[20].

1.5.7. Phosphatase and Tensin Homologue gene (*PTEN*)

The phosphatase and tensin homologue gene (*PTEN*) is also part of a growth-inducing signaling pathway, the PI3K/AKT pathway[47]. Contrarily to *EGFR*, *PTEN* is a tumor suppressor gene and, as such, *PTEN* inactivation is present in 20-30% of GBM[27]. However, relevance of these alterations in diagnosis, prognosis and response to therapy in glioma molecular subgroups has not been widely reported. A previous study by our group showed that *PTEN* deletion was more frequent in GBM *IDH*-wildtype and had a dual effect in glioma prognosis – favorable prognosis in GBM *IDH*-wildtype and unfavorable

prognosis in astrocytoma *IDH*-wildtype[29]. With all facts considered, routine assessment of this gene is not indicated[27].

Even though all of the potential molecular biomarkers discussed above have shown promise and have been heavily discussed in the last few years, most of them were not included in the 2016 WHO classification of CNS tumors and do not show advantages in routine testing[13,20,27].

1.5.8. Phosphatidylinositol-4,5-bisphosphate 3-kinase Catalytic Subunit Alpha gene (*PIK3CA*)

The phosphatidylinositol-4,5-bisphosphate 3-kinase catalytic subunit alpha gene (*PIK3CA*), located on chromosome 3q26, with 21 exons, codes for the p110α subunit of phosphatidylinositol-4,5-bisphosphate 3-kinase (PI3K), a key player in the PI3K/protein kinase B (AKT) pathway[47]. Among all the molecular alterations that lead to the deregulation of this pathway in cancer, *PIK3CA* mutations are the most prevalent[48]. *PIK3CA* somatic activating mutations are implicated in the constitutive activation of the PI3K/AKT pathway, independent from upstream signaling, and have been detected in various types of cancer, including breast cancer, colorectal cancer, ovarian cancer and glioma[49,50]. Indeed, these oncogenic mutations promote growth factor-independent growth, angiogenesis and resistance to apoptosis, and are thus involved in tumor progression and maintenance[47,48,50].

In breast cancer, there is high incidence of *PIK3CA* mutations in estrogen receptor (ER) positive, human epidermal growth factor receptor-2 (HER2) negative and metastatic tumors (~40%), with the association between these alterations and clinical outcome or response to therapy still controversial[51,52]. On the other hand, in colorectal cancer, these mutations have been associated with resistance to anti-EGFR therapy, as well as with increased risk for recurrence and poor prognosis[47].

In human cancer, the most frequent *PIK3CA* mutations are single amino acid substitutions – E545K and E542K at exon 10 (previously designated as exon 9) and H1047R at exon 21 (previously designated as exon 20)[51]. Exon 10 (according to Ensembl Transcript ID: ENST00000263967.4, RefSeq: NM_006218.4) encodes the p110α helical domain, responsible for the interaction between the catalytic subunit and the p85 regulatory subunit[49]. Thus, mutations in this region disrupt this interaction and prevent the catalytic subunit from being negatively regulated[50]. Exon 21 (according to Ensembl Transcript ID: ENST00000263967.4, RefSeq: NM_006218.4) codes for the p110α catalytic domain. In this case, the H1047R mutation increases the interaction between the catalytic domain and the plasma membrane, enhancing p110α's enzymatic activity[49,50]. Coexistence of two distinct *PIK3CA* mutations results in a synergistic effect, increasing their tumorigenic potential[53,54]. An *in vitro* study suggests that *PIK3CA* mutations promote astrocyte growth, but only H1047R induces colony formation in soft agar[55]. Conversely, an *in vivo* study identified the H1047R mutation as one of the main drivers of gliomagenesis, crucial in the modulation of the neuronal microenvironment to allow for malignant growth[56]. These results might indicate that this specific hotspot mutation induces a more aggressive phenotype in glioma. However, no study has made the correlation between type of mutation and clinical

prognosis in glioma thus far. In breast cancer patients, on the other hand, mutations in exon 21 are associated with worse outcomes[52].

In GBM, the frequency of *PIK3CA* mutations ranges from 5% to 30%[57–62]. Broderick et al. reported that only 5% (5/105) of GBM from the cohort analyzed were mutated for *PIK3CA*, having only analyzed exons 10 and 21 of this gene[57]. On the other hand, Samuels et al. sequenced the entire *PIK3CA* gene and found mutations in 27% (4/15) of GBM samples[58]. However, the cohort analyzed was much smaller. Additionally, Gallia et al. performed a multi-exon analysis and found that 18% (7/38) of adult primary GBM harbored *PIK3CA* mutations[59]. More recently, Lee et al. reported a *PIK3CA* mutation frequency of 30% (9/30) when considering multifocal GBM only, and 10% (13/130) when considering solitary GBM[61].

Fewer studies were performed regarding other glioma histological subgroups. Nevertheless, Broderick et al. reported mutations in 14% (3/21) of oligodendrogliomas and 3% (1/31) of astrocytomas[57]. In another study, Hartmann et al. analyzed exons 1, 10 and 21 and found *PIK3CA* mutations in 5% (3/66) of oligodendrogliomas[63]. Lastly, in a genome-wide analysis, the Cancer Genome Atlas (TCGA) network reported a frequency of 20% (17/84) mutations in 1p/19q codeleted, *IDH*-mutant oligodendrogliomas[41].

The disparities seen across many studies in regards to *PIK3CA* mutation frequencies in glioma can be associated with the subgroups analyzed, sample size, techniques used to identify the mutations and whether *PIK3CA* was analyzed in its entirety or only specific mutational hotspots were taken into account[64].

Only one of the mentioned studies evaluated the frequency of *PIK3CA* mutations considering the glioma molecular subgroups defined by the 2016 WHO classification of CNS tumors – in this case, only in 1p/19q codeleted, *IDH*-mutant gliomas[41]. Furthermore, the prognosis value of *PIK3CA* mutations in glioma is still very unclear. Previously by our group, the impact of *PIK3CA* mutations in exons 10 and 21 on glioma molecular subgroups was investigated, in a cohort from Instituto Português de Oncologia de Lisboa Francisco Gentil (IPOLFG) (n=403) and a cohort from TCGA (n=592). These mutations were found in 3% of GBM *IDH1*-wildtype, 9% of GBM *IDH*-mutant, 9% of astrocytoma *IDH1*-wildtype, 5% of astrocytoma *IDH*-mutant, and 10% of oligodendroglioma *IDH*-mutant and 1p/19q-codeleted. Results were corroborated with TCGA data for the GBM subgroup, where GBM *IDH*-mutant continued to present a higher frequency of *PIK3CA* mutations in these exons than GBM *IDH*-wildtype (8% versus 2%, respectively). However, one of the limitations of this study was that glioma samples were segregated regarding *IDH1* mutational status only[65].

Furthermore, our group also evaluated if *PIK3CA* mutations were a prognostic factor in GBM *IDH*-wildtype patients, the most representative group of the IPOLFG cohort. Results showed that *PIK3CA* mutations in exons 10 and 21 had no significant prognosis value in this molecular subgroup[66]. Moreover, multivariable analysis of the TCGA cohort corroborated these results, as *PIK3CA* molecular alterations were not independent prognostic factors[66].

Regarding other studies, evidences suggest that patients with *PIK3CA* mutated multifocal GBM have worse prognosis than patients with wildtype *PIK3CA*[61]. Another study shows that, in a multivariate

analysis, *PIK3CA* mutations were associated with a decrease in Progression Free Survival, in patients with GBM *IDH1*-wildtype[62]. Furthermore, these mutations were also associated with a more disseminated phenotype, i.e. widespread disease[62].

Most importantly, *PIK3CA* mutations have been described as early and constitutive events in glioma development, present in all sectors of the tumor[61]. Considering that gliomas, and particularly GBM, are very heterogenous tumors, this could mean that *PIK3CA* mutations represent a promising therapeutic target[61]. Indeed, the analysis of recurrence cases in the IPOLFG cohort indicated that *PIK3CA* mutations constitute early events that remain through glioma progression regardless of the therapy administered[66]. Therefore, these results may also suggest that these alterations play a role in therapy resistance. Notably, the E545K mutation has shown to confer radioresistance to tumor cells, in cervical cancer[67].

Still, the impact of *PIK3CA* mutations in the diagnosis, prognosis and response to therapy of glioma molecular subgroups remains unclear, highlighting the need for further research.

1.6. The PI3K/AKT signaling pathway

The PI3K/AKT signaling pathway plays a crucial role in the regulation of numerous essential biological processes, such as cell proliferation, survival, metabolism, motility, apoptosis and angiogenesis[47,64]. Class I PI3K is a lipid kinase responsible for the phosphorylation of phosphatidylinositol-4,5-bisphosphate (PIP_2) to phosphatidylinositol-3,4,5-triphosphate (PIP_3) when activated by upstream receptor tyrosine kinases (e.g. EGFR) or G protein-coupled receptors through binding of growth factors, cytokines or hormones[50,64] (**Figure 1.4**). PIP_3, which accumulates in the plasma membrane, will in turn activate AKT through recruitment of phosphatidylinositol-dependent kinases (PDK)[51]. Activated AKT is one of the main players in this pathway, responsible for the phosphorylation of various downstream targets. One of the main branches of this signaling involves the release of mechanistic target of rapamycin complex 1 (mTORC1) inhibition upon tuberculosis sclerosis complex 2 (TSC2) phosphorylation[68,69]. Thus, AKT indirectly activates mechanistic target of rapamycin (mTOR), culminating in cell death inhibition and promoting cell survival, growth and angiogenesis[47,51]. Tumor suppressor PTEN is the negative regulator of this pathway, responsible for dephosphorylating PIP_3 back to PIP_2[47].

PI3K kinases are divided into three main classes depending on structure, function and substrate specificity[47]. Class I PI3K is the most studied, with the mechanism of action detailed above. It is a heterodimeric kinase, composed of a catalytic subunit, p110, and a regulatory subunit, p85[50]. This class is further divided into two subclasses – IA and IB. Class IA PI3K contains the catalytic subunits p110α, p110β and p110δ, encoded by *PIK3CA*, *PIK3CB* and *PIK3CD*, respectively[49]. Class IB PI3K only contains the p110γ catalytic subunit, encoded by *PIK3CG*[47]. The main difference between all these catalytic subunits is their regulation and cellular localization – p110α and p110β are distributed throughout all human tissues, whereas p110δ and p110γ are mainly present in leukocytes[47,64].

As opposed to Class I PI3K, Class II PI3K are monomeric kinases that have been shown to be more involved in angiogenesis regulation, through a mechanism still not well established[50,64]. Finally, Class III PI3K are multisubunit kinases linked to autophagy regulation[50].

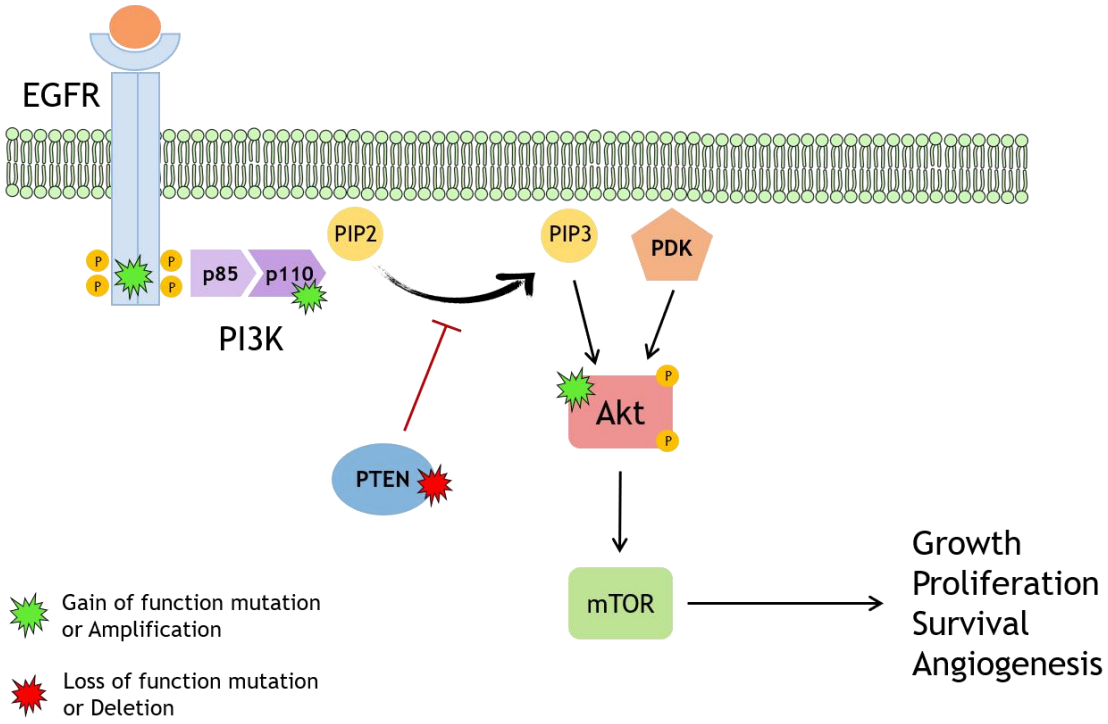

Figure 1.4. Simplified schematic representation of the PI3K/AKT pathway. Binding of ligand to a receptor tyrosine kinase, e.g. EGFR, triggers the phosphorylation of PIP_2 to PIP_3 by class I PI3K. In turn, PIP_3 recruits PDK in order to activate AKT. AKT is responsible for the activation of various downstream effectors, including mTOR, ultimately promoting cell growth, proliferation, survival and angiogenesis. PTEN is the negative regulator of this pathway, catalyzing the conversion of PIP_3 to PIP_2. Important alterations in this pathway that promote tumorigenesis are highlighted in green and red. EGFR, epidermal growth factor receptor; PI3K, phosphatidylinositol-4,5-bisphosphate 3-kinase; AKT, protein kinase B; PIP_2, phosphatidylinositol-4,5-bisphosphate; PIP_3, phosphatidylinositol-3,4,5-triphosphate; PDK, phosphatidylinositol-dependent kinases; mTOR, mechanistic target of rapamycin; PTEN, phosphatase and tensin homologue

Class IA PI3K has been shown to be clearly implicated in many human cancer types[49]. The PI3K/AKT pathway is seen as one of the main pathways deregulated in cancer[50]. It is known to play a central role in tumorigenesis and cancer progression, most notably in breast cancer but also in GBM[51,64]. Its overactivation is usually attributed to somatic activating mutations or amplifications in genes promoting this signaling, such as *EGFR* and *PIK3CA*, or loss of its antagonist, *PTEN*[49]. All these molecular alterations lead to the constitutive activation of the PI3K/AKT pathway, and consequently to excessive proliferation and apoptosis inhibition. Therefore, the PI3K/AKT pathway is considered a promising therapeutic target in cases where it is upregulated[50].

1.7. Targeted inhibition of PI3Kα

PI3K has been considered a relevant therapeutic target in many cancers due to its important role in tumorigenesis and cancer progression, as discussed previously[53]. Its inhibition has the potential to

reduce cell proliferation and angiogenesis while promoting cell death[49]. As a consequence, various class IA PI3K inhibitors have been developed through the years and are currently undergoing clinical trials[53]. However, results have shown limited efficiency of these inhibitors in tumors harboring upregulation of the PI3K/AKT pathway, mainly due to acquired resistance and poor tolerability[50]. Two main mechanisms of resistance have been observed – the activation of compensatory pathways (e.g. extracellular signal-regulated kinase (ERK) and Wnt-β-catenin) and acquired mutations in regulatory genes[70]. Furthermore, different PI3K isoforms have proven to play different, non-redundant roles in human cancer[50]. More efficient therapeutic strategies could thus include combination therapies and isoform selective inhibitors, which are currently being developed[53,71]. Indeed, isoform selective PI3K inhibitors have generally shown more promising and efficient results with fewer toxicity and off-target effects[70].

BYL719, also known as alpelisib, is a selective isoform inhibitor from the 2-aminothiazole class that binds to the adenosine triphosphate (ATP) pocket of the p110α catalytic subunit kinase domain[72]. Therefore, it is highly specific for PI3Kα[53]. This inhibitor has been shown to exhibit a dose-dependent antitumor activity, more pronounced in the presence of *PIK3CA* mutations and with heightened sensitivity in the presence of double mutations[54,71–73]. Hence, *PIK3CA* mutations could be predictive of a better response to alpelisib treatment, making this compound a promising therapeutic drug in patients with mutant *PIK3CA* and highlighting the need to add this molecular biomarker to routine testing[53,71].

Alpelisib is already in phase I/II clinical trials for breast cancer, lung cancer, pancreatic cancer and squamous cell carcinoma[71]. *PIK3CA* mutant and ER-positive patients that received a combination of alpelisib plus fulvestrant (selective estrogen receptor degrader) showed an increase in progression free survival, when compared to *PIK3CA* wildtype patients[70]. Alpelisib side effects included hyperglycemia, nausea, decreased appetite, diarrhea and vomiting[53]. Another trial involving patients with *PIK3CA*-altered solid tumors received daily doses of alpelisib, which demonstrated a tolerable safety profile and signs of antitumor activity[74]. As a result, this drug was recently approved for treatment of ER-positive, HER2-negative and *PIK3CA*-mutated breast cancer patients, in combination with fulvestrant[73].

The effect of PI3K inhibition in *PIK3CA* mutant gliomas has been less explored. Buparlisib, which is considered a pan-PI3K inhibitor that can cross the blood-brain barrier, is the most frequent PI3K inhibitor used in GBM clinical trials[71]. However, patients harboring *PIK3CA* mutations do not seem to benefit from this treatment[71,75]. A study using normal human astrocytes transfected with hotspot *PIK3CA* mutations showed that these mutations did not enhance the effect of buparlisib[55]. Nevertheless, treatment with an isoform selective inhibitor, such as alpelisib, could yield different results. So far, no clinical trials for this inhibitor have been carried out with GBM patients[71].

1.8. Objectives

Considering the vast potential that *PIK3CA* mutations hold as promising therapeutic targets in glioma, as well as the recent breakthroughs concerning alpelisib as an effective therapeutic strategy in

breast cancer, the main goal of this work is to evaluate the *in vitro* inhibition of PI3Kα in glioma cell models harboring hotspot *PIK3CA* mutations. More specifically, this work aims to:

(1) Search for *IDH2* mutations in the IPOLFG glioma cohort, particularly in the GBM *IDH1*-wildtype and astrocytoma *IDH1*-wildtype subgroups. Even though *IDH2* mutations are much rarer, this analysis will help better characterize this cohort and produce more accurate results regarding the frequency of *PIK3CA* mutations in glioma molecular subgroups;

(2) Explore the relationship between *PIK3CA* mutations/expression and the glioma immune microenvironment, using *in silico* analysis;

(3) Successfully transfect distinct cell models in order to harbor the *PIK3CA* hotspot mutations E545K and H1047R;

(4) Evaluate the impact that distinct *PIK3CA* mutations might have on clonogenicity, cell migration and invasion of different glioma cell models;

(5) Assess the effect of alpelisib and TMZ on the activation of the PI3K/AKT pathway, as well as on cell viability, proliferation and death, in the presence of *PIK3CA* hotspot mutations.

2. Material and Methods

2.1. Biological samples

A cohort of 403 adult diffuse gliomas, diagnosed from 2011 to 2016, referred to Unidade de Investigação em Patobiologia Molecular of Instituto Português de Oncologia de Lisboa Francisco Gentil (IPOLFG) was previously reclassified by our group[29] according to the 2016 WHO classification of CNS tumors[13]. This cohort included 245 GBM *IDH1*-wildtype, 11 GBM *IDH*-mutant, 43 astrocytoma *IDH1*-wildtype, 55 astrocytoma *IDH*-mutant and 49 oligodendroglioma *IDH*-mutant and 1p/19q codeleted samples. DNA was previously extracted from frozen or paraffin-preserved tissue and diluted to 80 ng/µL, as described in Brito et al[29]. However, in previous work the mutational status of *IDH2* was not evaluated. Herein, samples with unknown *IDH2* mutational status – GBM *IDH1*-wildtype and astrocytoma *IDH1*-wildtype subgroups – were analyzed. Six GBM *IDH1*-wildtype and three astrocytoma *IDH1*-wildtype samples were excluded due to lack of biological material. This study was previously approved by the IPOLFG Ethical Board Committee (UIC/1203). As it is a retrospective study, written informed consent was obtained from all living patients.

2.2. *IDH2* hotspot mutation analysis

In order to evaluate the presence of the R172 hotspot mutation in exon 4 of *IDH2* in the previously established glioma molecular subgroups, this region was amplified by Polymerase Chain Reaction (PCR), using forward primer 5' AATTTTAGGACCCCCGTCTG 3' and reverse primer 5' CTGCAGAGACAAGAGGATGG 3'. PCR was performed in a final volume of 12.5 µL**,** containing 80 ng of sample DNA, 1.25 µL Hi-Fi Buffer (1x), 0.2 µM deoxyribonucleotides, 6 mM $MgCl_2$, 0.32 µM forward and reverse primers and 0.4 U Platinum™ Taq DNA Polymerase High Fidelity (all reagents obtained from Invitrogen, Thermo Fisher Scientific, USA). The reaction was carried out in a Biometra® T3 Thermocycler and consisted of an initial denaturation step at 96 ºC for 5 minutes, followed by 35 cycles of denaturation (95 ºC for 30 seconds) - annealing (64 ºC for 40 seconds) - extension (72 ºC for 50 seconds), and a final extension step at 72 ºC for 10 minutes. The length of the obtained amplicon was 345 base pairs.

After amplification, samples were subjected to gel electrophoresis in 2% agarose gel in Tris/Borate/Ethylenediaminetetraacetic acid (EDTA) (TBE) buffer 1x (VWR, USA), stained with 0.5 µg/mL ethidium bromide (PanReac Applichem, Spain), which was visualized under UV radiation to verify PCR amplification.

Next, PCR products were purified by enzymatic digestion with 20 U exonuclease I and 2 U FastAP Thermosensitive Alkaline Phosphatase (both from Thermo Fisher Scientific, USA). The reaction consisted of two steps – a digestion step for 15 minutes at 37 ºC to ensure optimal enzymatic activity, and an inactivation step at 85 ºC for 15 minutes.

Lastly, PCR products were sequenced using the automatic sequencer ABI Prism 3130 Genetic Analyzer (Applied Biosystems, Thermo Fisher Scientific, USA), according to the instructions proposed by Big Dye™ Terminator v1.1 Cycle Sequencing Kit (Applied Biosystems, Thermo Fisher Scientific, USA). The sequencing reaction was performed in a final volume of 20 µL, containing 2 µL Big Dye™

Terminator v1.1 Sequencing Buffer, 0.17 µM forward primer, 0.75 µL Big Dye™ Terminator v1.1 Ready Reaction Mix and 3 µL of purified PCR product. The reaction consisted of an initial denaturation step at 96 ºC for 5 minutes, followed by 25 cycles of denaturation (95 ºC for 10 seconds) - annealing (58 ºC for 15 seconds) - extension (60 ºC for 4 minutes), performed in a Biometra® T3 Thermocycler. The sequencing reaction was purified by ethanol/EDTA/sodium acetate precipitation. EDTA, sodium acetate and ethanol were added to the total volume of sequencing reaction, in a final concentration of 3.8 mM, 80 mM and 70% (v/v), respectively. After centrifugation at 20800 g, for 30 minutes at 4 ºC, pellets were resuspended in 70% (v/v) ethanol, followed by another centrifugation at 20800 g, for 15 minutes at 4 ºC. Pellets were dried at 37 ºC, for 10 minutes, and resuspended in 20 µL of Hi-Di™ Formamide (Applied Biosystems, Thermo Fisher Scientific, USA) before being introduced into the automatic sequencer.

2.3. *In silico* analysis

The relationship between *PIK3CA* mutations and the infiltration of B lymphocytes, Cluster of Differentiation 4 positive (CD4+) and CD8+ T cells, neutrophils, macrophages, and dendritic cells in GBM and low-grade gliomas (LGG) was evaluated using the bioinformatic tool Tumor Immune Estimation Resource (TIMER)[76]. The correlation between *PIK3CA* expression and the expression of various immune cell gene markers for B lymphocytes, dendritic cells, macrophages, microglia, monocytes, Natural Killer (NK) cells, neutrophils, tumor-associated macrophages (TAM), CD8+ T cells, T helper cells, regulatory T cells (Tregs), and T cell exhaustion was also assessed using TIMER.

2.4. Cell culture and transfection

Human GBM cell line U87MG, obtained from American Type Cell Collection (ATCC), was cultured in Dulbecco's modified Eagle's medium (DMEM), supplemented with 10% fetal bovine serum (FBS) and 1% penicillin/streptomycin (P/S) (all from Gibco, Thermo Fisher Scientific, USA). Normal human astrocytes (Lonza, Switzerland) were previously immortalized in the lab, through the introduction of the simian virus 40 T antigen gene (kind gift from José Ramalho, CEDOC), originating immortalized normal human astrocytes (iNHA). These cells were cultured in DMEM F-12 (BioWhittaker, Lonza, Switzerland), supplemented with 10% FBS and 1% P/S. Both cell lines were kept in a humidified atmosphere incubator, at 37 ºC with 5% (v/v) CO_2.

Cells were transfected with the following plasmids: PIK3CA-WT (Addgene plasmid #16643; http://n2t.net/addgene:16643; RRID: Addgene_16643), PIK3CA-E545K (Addgene plasmid #16642; http://n2t.net/addgene:16642; RRID: Addgene_16642) and PIK3CA-H1047R (Addgene plasmid #16639; http://n2t.net/addgene:16639; RRID: Addgene_16639), which were a gift from Bert Vogelstein[58]. Transfection was performed with Lipofectamine™ 2000 Transfection Reagent (Invitrogen, Thermo Fisher Scientific, USA), following manufacturer's instructions. Briefly, U87MG and iNHA cells were seeded in 6-well plates at a density of $2.5x10^5$ cells/well. After 24 hours, plasmid DNA was diluted to desired quantity (1-4 µg) in 500 µL of serum free media. 20-30 µL of Lipofectamine™ 2000 Transfection Reagent were also diluted in 500 µL of serum free media. Plasmid DNA was added to the

diluted Lipofectamine™, and incubated for 20 minutes, at room temperature. Then, the DNA-Lipofectamine™ mix was added to the cells, followed by a 5-hour incubation period at 37 ºC with 5% (v/v) CO_2. After incubation, cell culture media with 10% FBS and 1% P/S was added.

Stable U87MG and iNHA transfectants were selected in the presence of 500 µg/mL and 250 µg/mL geneticin (PanReac Applichem, Spain), respectively, for 3 weeks. Cells were also treated with geneticin every 10th passage, to ensure proper selection.

2.4.1. Transfection validation

The presence of both mutations, E545K and H1047R, in both cell lines was confirmed by Sanger sequencing of cDNA. Briefly, total RNA was extracted and purified from cultured cells using NZY Total RNA Isolation kit (NZYTech, Portugal) according to manufacturer's instructions, and quantified using Nanodrop 2000 (Thermo Fisher Scientific, USA). Then, cDNA was synthesized from 1 µg of total RNA using either NZY First-Strand cDNA Synthesis kit (NZYTech, Portugal) or SuperScript™ III Reverse Transcriptase (Invitrogen, Thermo Fisher Scientific, USA), following the provided protocols.

Exons 10 and 21 of *PIK3CA* were amplified by PCR, using cDNA as template. Exon 10 was amplified using forward primer 5' TGTATCCCGAGAAGCAGGAT 3' and reverse primer 5' GAATTTCGGGGATAGTTACACAA 3', generating a 197 base pair fragment whilst exon 21 amplification was achieved using forward primer 5' ATGATGCTTGGCTCTGGAAT 3' and reverse primer 5' TGTGTGGAAGATCCAATCCAT 3', producing a 174 base pair amplicon. PCR was performed in a final volume of 10 µL, containing 3 µL of template cDNA at 20 µg/µL, 5 µL AmpliTaq Gold™ 360 Master Mix (Applied Biosystems, Thermo Fisher Scientific, USA) and 1 µM forward and reverse primers (Invitrogen, Thermo Fisher Scientific, USA). The reaction was carried out in a Biometra® T3 Thermocycler and consisted of an initial denaturation step at 95 ºC for 5 minutes, followed by 35 cycles of denaturation (95 ºC for 5 seconds) - annealing (61 ºC for 30 seconds) - extension (72 ºC for 1 minute), and a final extension step at 72 ºC for 5 minutes. PCR products were purified by enzymatic digestion and sequenced as described in Section 2.2, with modifications to the sequencing reaction, which contained 3.5 µL Big Dye™ Terminator v1.1 Sequencing Buffer, 2 µM forward primer, 2 µL Big Dye™ Terminator v1.1 Ready Reaction Mix and 10 µL of purified PCR product.

Furthermore, *PIK3CA* and *PIK3CA* mutations expression was assessed by Real-Time reverse transcriptase quantitative PCR (RT-qPCR), using forward primer 5' ACGTGTGCCATTTGTTTTGA 3' and reverse primer 5' GATTGGCATGCTGTCGAATA 3'. *HPRT1* was the housekeeping gene used as endogenous control, amplified with forward primer 5' TGACACTGGCAAAACAATGCA 3' and reverse primer 5' GGTCCTTTTCACCAGCAAGCT 3'. The reaction was carried out in a QuantStudio 5 Real-Time PCR System (Applied Biosystems, Thermo Fisher Scientific, USA), in a final volume of 20 µL, containing 2 µL of cDNA, SYBR™ Green PCR Master Mix 0.5x (Applied Biosystems, Thermo Fisher Scientific, USA) and 0.25 µM forward and reverse primers (Invitrogen, Thermo Fisher Scientific, USA). Real-Time PCR conditions were as follows: 2 minutes at 50 ºC followed by 10 minutes at 95 ºC; then 41 cycles of denaturing at 95 ºC for 15 seconds and annealing/extension at 60 ºC for 1 minute; lastly

heating to 95 ºC for 15 seconds for final denaturation step. Relative quantification of *PIK3CA* gene expression was obtained with the ΔΔCt method, as previously described[77].

2.5. Colony formation assay

U87MG transfected cells were seeded in triplicates, in 6-well plates, at a density of 700 cells/well. Colonies were allowed to form for 10 days, at which point they were fixed with cold methanol for 5 minutes and stained with 0.5% crystal violet. Four independent assays were performed and the number of colonies per well was manually quantified.

2.6. Cell migration and invasion

Cell migration was assessed using Falcon® Permeable Cell Culture Inserts for 24-well Plate with 8.0 µm Transparent PET Membrane (Corning, USA). Cell invasion was determined using Corning® Matrigel® Invasion Chambers for 24-well Plate with 8.0 µm Transparent Polyethylene Terephthalate (PET) Membrane (Corning, USA), following manufacturer's instructions. U87MG cells were seeded into both cell culture inserts, at a density of $5x10^4$ cells/well in DMEM with 5% FBS and 1% P/S, whilst the lower chambers were filled with DMEM with 10% FBS, 20 ng/mL epidermal growth factor (EGF) and 1% P/S.

Plates were incubated for 24 hours in a humidified atmosphere, at 37 ºC with 5% (v/v) CO_2. Cells that did not migrate or invade were removed from the inserts using a cotton-tipped applicator. Cells that migrated through the membrane or invaded through the Matrigel to the membrane were then fixed with cold methanol for 5 minutes and stained with Vectashield® Antifade Mounting Medium with DAPI (Vector Laboratories, USA).

To calculate the number of migrating or invading cells, 10 pictures were acquired per insert, at 100x magnification, with an inverted fluorescence microscope and the total number of cells was quantified using ImageJ version 1.52p.

2.7. Cell viability

Using both U87MG and iNHA cells, TMZ half-maximal inhibitory concentration (IC_{50}) was determined by Cell Counting Kit-8 (CCK8; Dojindo, Japan). Briefly, $1.6x10^4$ cells/well or $4x10^3$ cells/well were seeded in triplicates, in 24-well plates. After 24 hours, cells were exposed to vehicle (dimethyl sulfoxide 1% – DMSO) or different TMZ (Sigma-Aldrich, Merck, Germany) concentrations (10, 50, 100, 200, 400, 600, 800 µM) for 3 or 6 days, respectively. Then, CCK8 was added to each well in a 1:10 dilution, followed by a 30-minute incubation period at 37 ºC with 5% (v/v) CO_2, in the dark. Absorbance values were measured at 450 nm in a 96-well plate, using the iMark™ Microplate Absorbance Reader (BioRad, USA). The same protocol was used to determine alpelisib (Selleck Chemicals, USA) IC_{50}, using the concentrations 1, 5, 10, 15, 25, 50, 100 µM. Culture media with vehicle, TMZ or alpelisib was renewed at day 3.

Cell viability was also assessed in U87MG transfected cells after treatment with vehicle, TMZ (300, 600 µM) or alpelisib (7, 15 µM), using the same methodologies.

For the Trypan blue assay (Gibco, Thermo Fisher Scientific, USA), $2x10^4$ cells/well were seeded in 6-well plates. After 24 hours, cells were exposed to vehicle (DMSO 1%), TMZ (300, 600 µM) or alpelisib (7, 15 µM), for 3 or 6 days. Then, cells were trypsinized to create a cell suspension, which was mixed with Trypan blue (1:1 ratio). Viable cells were counted with a hemocytometer under the microscope. Culture media with vehicle, TMZ or alpelisib was renewed at day 3.

2.8. Cell death

U87MG transfected cells were seeded in 12-well plates at a density of $3.2x10^4$ cells/well or $8x10^3$ cells/well. After 24 hours, cells were exposed to vehicle (DMSO 1%), TMZ (0, 300, 600 µM) or alpelisib (0, 7, 15 µM), for 3 or 6 days, respectively. Cells were trypsinized and centrifuged at 150 g, for 5 minutes. Then, cells were washed with phosphate-buffered saline, bovine serum albumin (PBS-BSA) 0.1% and centrifuged again at 150 g, for 2 minutes. FITC Annexin V (BioLegend, USA) was added to the cells in annexin binding buffer (0.01 M HEPES, 0.14 M NaCl, 2.5 mM $CaCl_2$), followed by a 15-minute incubation in the dark. PBS-BSA 0.1% was added, and cells were centrifuged once more at 150 g, for 2 minutes. Annexin binding buffer was added to each sample, as well as Propidium Iodide (PI) right before flow cytometry analysis. A total of at least 10000 events were acquired and the results analyzed in FlowJo software (version 10). Culture media with vehicle, TMZ or alpelisib was renewed at day 3.

2.9. Western Blot

U87MG transfected cells were seeded in T25 flasks at a density of $2.5x10^6$ cells/flask. Without treatment, these cells were collected 3 days after seeding. With treatment, 24h after seeding, cells were exposed to vehicle (DMSO 1%), TMZ (300, 600 µM) or alpelisib (7, 15 µM) for 3 days. Cells were washed with PBS, scraped, and lysed for 1 hour using ice-cold radioimmunoprecipitation assay (RIPA) lysis buffer (Thermo Fisher Scientific, USA) with 1:100 protease and phosphatase inhibitor cocktail (Sigma-Aldrich, Merck, Germany). After being centrifuged at 15000 g for 20 minutes, at 4ºC, the pellet was discarded and protein concentration was determined using the Pierce BCA protein assay kit (Thermo Fisher Scientific, USA), according to manufacturer's instructions. Using 10% and 12% sodium dodecyl sulfate (SDS)-polyacrylamide gels, protein extracts (40 µg) were separated by electrophoresis and transferred onto polyvinylidene difluoride (PVDF) membranes (BioRad, USA) using the Trans-Blot Turbo Transfer System (BioRad, USA). The membranes were blocked in PBS-BSA 5% Tween 0.1% for 1 h. The following primary antibodies were used, diluted in PBS-BSA 3% Tween 0.1%: anti-phospho-AKT (Thr308) (1:1000 dilution; overnight incubation; 13038 Cell Signaling Technology), anti-AKT (1:1000 dilution; overnight incubation; 4691 Cell Signaling Technology), anti-PTEN (1:500 dilution; 48h incubation; 9559 Cell Signaling Technology), anti-MMP2 (1:165 dilution; 72h incubation; 13132 Cell Signaling Technology), anti-MMP7 (1:165; 72h incubation; 3801 Cell Signaling Technology); anti-β-actin, clone AC-15 (1:5000 dilution; 1h incubation; A5441, Merck, Germany). Primary antibodies were detected using secondary horseradish peroxidase-conjugated goat anti-rabbit and anti-mouse antibodies (1:10000 dilution; 1h incubation; 31460 and 31430, Thermo Fisher Scientific, USA), using

Clarity Western ECL Substrate (BioRad, USA). Membranes were imaged by ChemiDoc XRS+ (BioRad, USA).

2.10. Statistical analysis

Differences between immune cell subsets in GBM and LGG were determined by Wilcoxon rank sum test. Spearman's rank correlation coefficients and respective *p*-values were obtained for all immune cell markers in both GBM and LGG.

IC_{50} values were calculated using a non-linear regression, based on a concentration vs. response variable slope, in GraphPad Prism version 8.4.3.

For RT-qPCR, t-tests were used to detect differences between 2 groups. For colony formation, migration and invasion assays, one-way analysis of variance (ANOVA) was used to compare between different groups of transfected cells, followed by Turkey's multiple comparisons test to compare individual means. A significance level of 5% was considered. For cell viability assays, two-way ANOVA was used to compare between different groups of transfected cells and different treatment concentrations, followed by Turkey's multiple comparisons test to compare individual means. A significance level of 5% was considered.

All statistical analyses and graphical representations were performed using GraphPad Prism version 8.4.3. Data are presented as mean ± standard error of the mean (SEM).

3. Results

3.1. *IDH2* mutational status in the IPOLFG glioma cohort

Our group had previously calculated the frequency of *PIK3CA* mutations in the IPOLFG glioma cohort[65]. However, since this cohort had been classified into molecular subgroups based solely on *IDH1* mutational status[29], the frequencies obtained could be slightly inaccurate. Thus, we searched for the R172 *IDH2* hotspot mutation in these samples, to better characterize the IPOLFG glioma cohort, as well as to provide more accurate *PIK3CA* mutation frequencies. *IDH1*-wildtype samples were sequenced, as *IDH1* and *IDH2* mutations are mutually exclusive[78]. Out of 279 glioma samples analyzed, only one harbored an *IDH2* R172 hotspot mutation (**Figure 3.1**). It corresponded to a sample previously classified as astrocytoma *IDH1*-wildtype. With the detection of the heterozygous R172M *IDH2* mutation (c.515G>T), this sample was reclassified as astrocytoma *IDH*-mutant, and the IPOLFG glioma cohort was rearranged with more accuracy. Nonetheless, as demonstrated in **Table 3.1**, this change was not profound enough to impact the frequency of *PIK3CA* mutations across the molecular subgroups, with it remaining unchanged. *IDH*-mutant and 1p/19q codeleted gliomas and astrocytomas *IDH*-wildtype remain the molecular subgroups with the highest *PIK3CA* mutation percentage (10%). Still, the overall frequency of *PIK3CA* mutations in the IPOLFG glioma cohort is relatively low (5%).

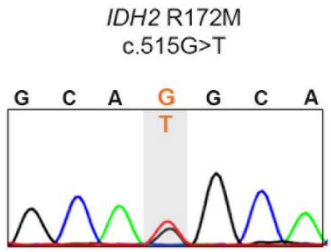

Figure 3.1. Sanger sequencing of the *IDH2* R172M mutation. The only sample that harbored an *IDH2* hotspot mutation in exon 4, belonging to the astrocytoma *IDH*-mutant subgroup, is represented. The altered nucleotide is highlighted.

As previously described[28,38,78], we also verified that *IDH1* mutations are undoubtedly more frequent than *IDH2* mutations in this cohort – in a total of 116 *IDH*-mutant glioma samples, 99% (115/116) of these alterations are located in *IDH1*, whilst only 1% (1/116) are present in *IDH2*.

Table 3.1. Differences in the molecular classification of samples from the IPOLFG glioma cohort before and after *IDH2* mutational analysis. The number of samples from all IPOLFG glioma molecular subgroups are represented, as well as *PIK3CA*, *IDH1* and *IDH2* mutation percentages (when relevant).

Before *IDH2* mutational analysis			**After *IDH2* mutational analysis**				
Glioma molecular subgroup	**Number of samples**	***PIK3CA* mutation frequency**	**Glioma molecular subgroup**	**Number of samples**	***IDH1* mutation frequency**	***IDH2* mutation frequency**	***PIK3CA* mutation frequency**
GBM *IDH1*-wildtype	239	3% (6/239)	**GBM *IDH*-wildtype**	239	---	---	3% (6/239)
GBM *IDH*-mutant	11	9% (1/11)	**GBM *IDH*-mutant**	11	100% (11/11)	---	9% (1/11)
Astrocytoma *IDH1*-wildtype	40	10% (4/40)	**Astrocytoma *IDH*-wildtype**	39	---	---	10% (4/39)
Astrocytoma *IDH*-mutant	55	5% (3/55)	**Astrocytoma *IDH*-mutant**	56	98% (55/56)	2% (1/56)	5% (3/56)
***IDH*-mutant + 1p/19q codeleted gliomas†**	49	10% (5/49)	***IDH*-mutant + 1p/19q codeleted gliomas†**	49	100% (49/49)	---	10% (5/49)
Total	394	5% (19/394)	**Total**	394	29% (115/394)	0.3% (1/394)	5% (19/394)

†Oligodendrogliomas

3.2. Association between immune cell infiltration and *PIK3CA* mutations in glioma

Even though *PIK3CA* mutations are not frequent in the IPOLFG glioma cohort, this gene might still be a promising therapeutic target for these patients, especially considering that gliomas are currently virtually incurable. Most notably, targeted inhibition of PIK3CA combined with fulvestrant led to an increase in the progression free survival of *PIK3CA* mutant and ER-positive breast cancer patients[70].

Previously, our group observed that, in the IPOLFG cohort, these mutations seem to be maintained during glioma progression regardless of the therapy administered, which might indicate that *PIK3CA* mutations confer an advantage to tumor cells that allows for their survival[66]. The tumor microenvironment (TME) has been shown to play a significant role not only in tumor growth and metastasis[79], but also in the development of chemo- and radiotherapy resistance[80,81]. Hence, we decided to explore the relationship between tumor microenvironment and *PIK3CA* mutations.

Using the bioinformatic tool TIMER, infiltration level estimates of assorted immune cell subsets were analyzed in *PIK3CA* wildtype and mutant LGG and GBM samples (**Figure 3.2**). Out of the six immune subsets analyzed in both populations, only CD8+ T cell infiltration levels were significantly higher in *PIK3CA* mutant LGG samples when compared to *PIK3CA* wildtype. In GBM, this difference was not statistically significant, indicating that this association is specific of, and possibly important in lower-grade gliomas.

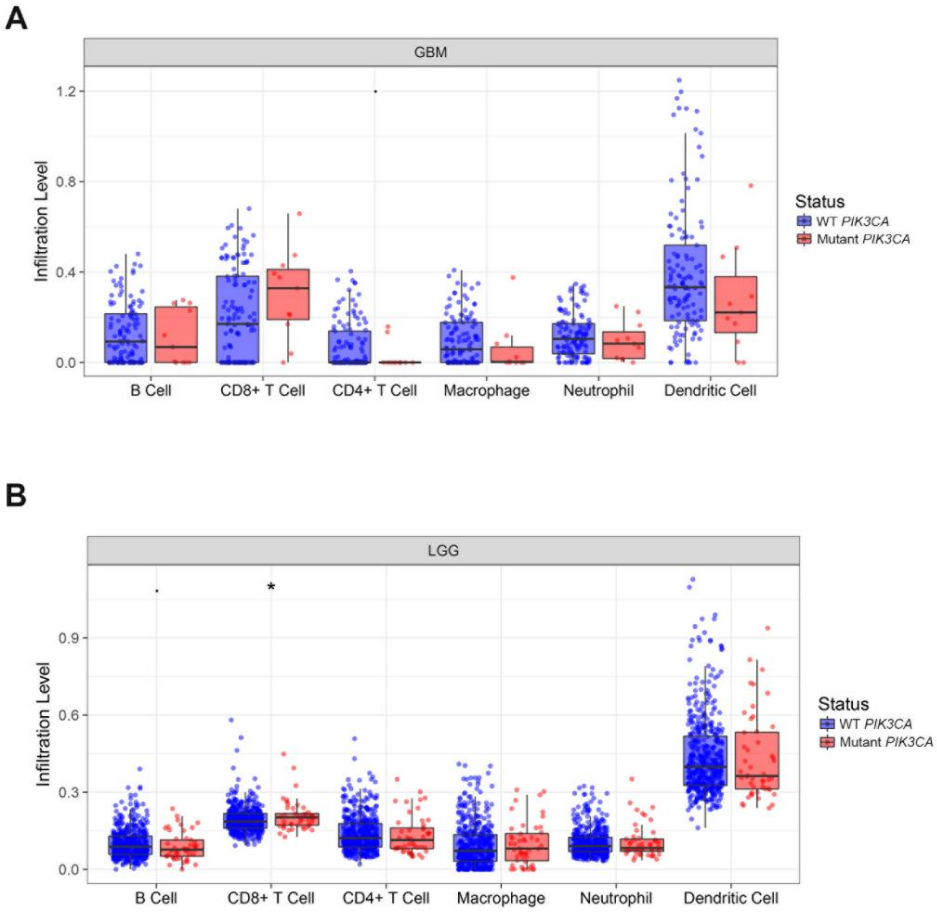

Figure 3.2. TIMER analysis of B cell, CD8+ T cell, CD4+ T cell, macrophage, neutrophil and dendritic cell infiltration in glioma samples harboring *PIK3CA* mutations. (**A**) Differences between infiltration levels of the distinct immune cell subsets in *PIK3CA* wildtype and *PIK3CA* mutant glioblastomas (GBM) (n=153). (**B**) Differences between infiltration levels of the same subsets in *PIK3CA* wildtype and *PIK3CA* mutant low-grade gliomas (LGG) (n=516). * $p<0.05$

Since *PIK3CA* mutations are activating and are thus associated with the constitutive activation of the PI3K/AKT pathway, we decided it would also be pertinent to assess the correlation between *PIK3CA* expression and the expression of distinct immune cell gene markers, both in GBM and LGG samples, using TIMER (**Table 3.2**). Out of a total of 63 gene markers analyzed, only *STAT5B*, a marker for regulatory T cells (Treg), showed a positive correlation with *PIK3CA* expression levels in LGG (cor=0.486; $p<0.001$), even after adjusting by tumor purity (cor=0.459; $p<0.001$). The same correlation was not found in GBM samples, and none of the other Treg markers analyzed had any correlation with *PIK3CA* expression.

Table 3.2. Correlation between *PIK3CA* expression and the expression of distinct immune cell gene markers. The data was obtained using the TIMER bioinformatic tool, including *p*-values and Spearman's rank correlation coefficients.

Description	Gene Marker	GBM				LGG			
		None		Purity		None		Purity	
		cor	*p*-value	cor	*p*-value	cor	*p*-value	cor	*p*-value
B cells	*CD19*	-0.152	0.06	-0.155	0.07	-0.105	0.017	-0.108	0.018
	CD79A	-0.143	0.079	-0.132	0.123	-0.082	0.062	-0.085	0.064
Dendritic cells	*HLA-DPB1*	-0.102	0.21	-0.04	0.644	-0.049	0.262	-0.028	0.542
	HLA-DQB1	0.111	0.17	0.147	0.087	-0.047	0.283	-0.023	0.619
	HLA-DRA	-0.166	0.041	-0.127	0.14	0.014	0.751	0.035	0.443
	HLA-DPA1	-0.112	0.169	-0.049	0.573	0.023	0.598	0.048	0.292
	BDCA1	-0.035	0.669	-0.003	0.968	0.077	0.08	0.093	0.042
	BDCA4	0.203	0.012	0.267	0.002	0.172	$9x10^{-5}$	0.163	$3x10^{-4}$
	CD11c	-0.164	0.043	-0.136	0.114	-0.243	$2.7x10^{-8}$	0.241	$9x10^{-8}$
M1 Macrophages	*INOS*	0.16	-0.049	0.191	0.025	-0.083	0.061	-0.072	0.117
	IRF5	-0.234	0.004	-0.23	0.007	-0.158	$3x10^{-4}$	-0.137	0.003
M2 Macrophages	*CD163*	0.141	0.083	0.224	0.009	0.236	$5.5x10^{-8}$	0.24	$1x10^{-7}$
	VSIG4	-0.072	0.375	0.003	0.973	0.105	0.017	0.13	0.004
	MS4A4A	-0.04	0.627	0.056	0.517	0.106	0.016	0.102	0.026
Microglia	*TMEM119*	-0.141	0.083	-0.073	0.397	-0.074	0.091	-0.034	0.458
	P2RY12	-0.196	0.015	-0.176	0.039	0.104	0.018	0.17	$1.9x10^{-4}$
	IBA1	-0.246	0.002	-0.229	0.007	-0.187	$2x10^{-5}$	-0.178	$9.5x10^{-5}$
	CX3CR1	-0.188	0.02	-0.162	0.059	0.052	0.237	0.105	0.022
Monocytes	*CD86*	-0.081	0.322	0	0.996	0.028	0.528	0.07	0.129
	CD115	0.026	0.75	0.128	0.135	0.04	0.361	0.091	0.047
NK cells	*KIR2DL1*	-0.038	0.643	0.012	0.894	0.083	0.06	0.09	0.05
	KIR2DL3	0.125	0.124	0.14	0.102	0.064	0.148	0.088	0.055
	KIR2DL4	-0.107	0.189	-0.096	0.264	0.068	0.122	0.077	0.092
	KIR3DL1	-0.009	0.91	0.011	0.899	0.081	0.066	0.079	0.084
	KIR3DL2	-0.033	0.69	0.006	0.948	0.009	0.841	0.023	0.611
	KIR3DL3	0.11	0.175	0.083	0.334	-0.023	0.605	-0.028	0.535
	KIR2DS4	-0.086	0.289	-0.062	0.473	0.06	0.173	0.087	0.059
	KLRK1	-0.043	0.594	-0.065	0.45	-0.009	0.832	-0.061	0.185
	NCR1	-0.002	0.985	0.008	0.927	0.116	0.008	0.114	0.013
	NCR2	-0.055	0.496	-0.053	0.542	0.068	0.121	0.087	0.057
	NCR3	-0.251	0.002	-0.245	0.004	-0.094	0.034	-0.071	0.123
Neutrophils	*CD66b*	0.079	0.331	0.091	0.29	0.014	0.757	0.008	0.854
	CD11b	0.054	0.503	0.138	0.107	0.001	0.988	0.049	0.282
	CCR7	-0.073	0.368	-0.024	0.78	0.06	0.172	0.079	0.084
TAM	*CCL2*	-0.188	0.02	-0.157	0.067	-0.016	0.715	0.005	0.912
	CD68	-0.08	0.328	-0.01	0.908	-0.027	0.543	-0.009	0.838
	IL10	-0.138	0.089	-0.063	0.464	-0.009	0.839	0	0.991
T cells (CD8+)	*CD8A*	-0.111	0.172	-0.086	0.319	-0.106	0.016	-0.028	0.546
	CD8B	-0.212	0.009	-0.201	0.018	-0.137	0.002	-0.083	0.071
T cells (general)	*CD3D*	-0.268	$8x10^{-4}$	-0.267	0.002	-0.071	0.011	-0.028	0.538
	CD3E	-0.149	0.067	-0.124	0.149	-0.042	0.344	-0.009	0.841

	CD2	-0.171	0.034	-0.146	0.088	-0.017	0.692	0.011	0.805
Th1	*TBX21*	0.009	0.914	0.012	0.893	-0.126	0.004	-0.126	0.006
	STAT4	-0.107	0.187	-0.059	0.491	-0.096	0.028	-0.033	0.478
	STAT1	-0.053	0.517	-0.039	0.648	0.23	$1.3x10^{-7}$	0.249	$3.6x10^{-8}$
	IFNG	0.034	0.68	0.024	0.779	-0.046	0.301	-0.02	0.667
	TNF	-0.225	0.005	-0.204	0.017	0.004	0.928	0.028	0.544
Th2	*GATA3*	0.118	0.145	0.163	0.057	-0.091	0.039	-0.08	0.081
	STAT6	0.001	0.992	0.058	0.499	-0.111	0.011	-0.016	0.722
	STAT5A	0.006	0.938	0.054	0.529	-0.12	0.006	-0.096	0.035
	IL13	-0.205	0.011	-0.224	0.009	-0.232	$9.6x10^{-8}$	-0.246	$5.4x10^{-8}$
Tfh	*BCL6*	0.26	0.001	0.273	0.001	0.273	$3.5x10^{-10}$	0.245	$5.9x10^{-8}$
	IL21	0.024	0.766	0.016	0.856	0.026	0.555	0.025	0.591
Th17	*STAT3*	0.169	0.037	0.188	0.028	0.311	$6x10^{-13}$	0.322	$5.6x10^{-13}$
	IL17A	0	1	0.008	0.93	-0.013	0.766	-0.012	0.79
Treg	*FOXP3*	-0.028	0.734	-0.005	0.951	-0.105	0.018	-0.1	0.029
	CCR8	-0.031	0.704	-0.011	0.902	0.012	0.783	0.009	0.849
	STAT5B	0.216	0.007	0.175	0.041	0.486	0	0.459	$2.8x10^{-26}$
	TGFB1	-0.057	0.482	-0.016	0.856	-0.165	$1.7x10^{-4}$	-0.144	0.002
T cell exhaustion	*PD1*	-0.04	0.625	0.025	0.769	-0.013	0.776	-0.002	0.97
	CTLA4	-0.066	0.419	-0.029	0.734	-0.068	0.122	-0.05	0.275
	LAG3	-0.058	0.472	-0.064	0.455	-0.136	0.002	-0.153	$7.8x10^{-4}$
	TIM3	-0.188	0.02	-0.146	0.09	-0.057	0.198	-0.028	0.539

NK, Natural Killer; TAM, tumor-associated macrophages; Th, T helper cells; Tfh, T follicular helper cells; Treg, T regulatory cells

3.3. Transfection of U87MG and iNHA with *PIK3CA* WT, E545K and H1047R

The next step was to understand the impact of *PIK3CA* mutations on glioma aggressiveness, by performing *in vitro* assays using glioma cell models. We chose two distinct cell models – U87MG cells, which are derived from GBM, and immortalized normal human astrocytes (iNHA), which somewhat mimic the behavior of LGG. Thus, our next goal was to transfect both glioma models with three distinct plasmids containing *PIK3CA* wildtype (WT), *PIK3CA* with the E545K mutation in exon 10 and *PIK3CA* with the H1047R mutation in exon 21. E545K and H1047R are the most common *PIK3CA* mutations, with the first affecting the helical domain of the p110α catalytic subunit of class IA PI3K, and the latter affecting the kinase domain (**Figure 3.3 A**).

Two attempts were made to transfect each cell line. First, the standard protocol used in the lab was executed – 20 µL of lipofectamine and 1 µg of plasmid DNA were added in each condition. However, this approach did not lead to a stable transfection and the expression of exogenous DNA was quickly lost, as proven by Sanger sequencing of cDNA (results not shown). Therefore, we tried to transfect both models once more, this time by changing both lipofectamine (20-30 µL) and plasmid DNA (1-4 µg) quantities added.

To validate this transfection, we first confirmed the presence of both mutations through Sanger sequencing of cDNA (**Figure 3.3 B-C**), to make sure that the desired alteration was being transcribed by the cells. In U87MG cells transfected with *PIK3CA* E545K and *PIK3CA* H1047R, the corresponding mutation was detected (**Figure 3.3 B**). However, the same was not verified for iNHA, in which cells

transfected with *PIK3CA* E545K or *PIK3CA* H1047R appeared wildtype for both mutations (**Figure 3.3 C**).

A second validation through RT-qPCR corroborated the previous results (**Figure 3.3 D-E**). In U87MG cells, the introduction of wildtype *PIK3CA* led to a 2.4-fold increase in the expression of this gene compared with the parental cell line (p=0.0154). Similarly, the introduction of *PIK3CA* E545K and *PIK3CA* H1047R resulted in a 3.1-fold and a 2.8-fold increase in *PIK3CA* expression, respectively (p=0.0243; p=0.0166) (**Figure 3.3 D**). Thus, transfection of U87MG cells with all three plasmids led to *PIK3CA* overexpression, as expected. However, similar results were not observed in iNHA cells (**Figure 3.3 E**). It is important to highlight that only two independent RT-qPCR assays were performed with iNHA transfected cells. Nonetheless, since we were unable to detect both E545K and H1047R mutations in the respective transfected cells, we concluded that iNHA transfection was unsuccessful and decided not to waste any more resources with additional validations.

U87MG cells were subjected to a third transfection validation through Western Blot, in order to verify if the altered gene expression would translate into an overactivation of the PI3K/AKT pathway (**Figure 3.3 F**). Indeed, the introduction of all three plasmids resulted in a slight increase in the levels of phosphorylated AKT (at position T308) when compared with the parental cell line. Despite these cells harboring a homozygous *PTEN* mutation, c.209+1G>T, which may decrease PTEN protein levels[82], transfection with all plasmids still resulted in higher PTEN levels, the main regulator of this pathway, which is consistent with a higher PI3K/AKT pathway activity. Since we were not able to successfully transfect iNHA after several attempts, we decided to proceed to *in vitro* assays with U87MG transfected cells only.

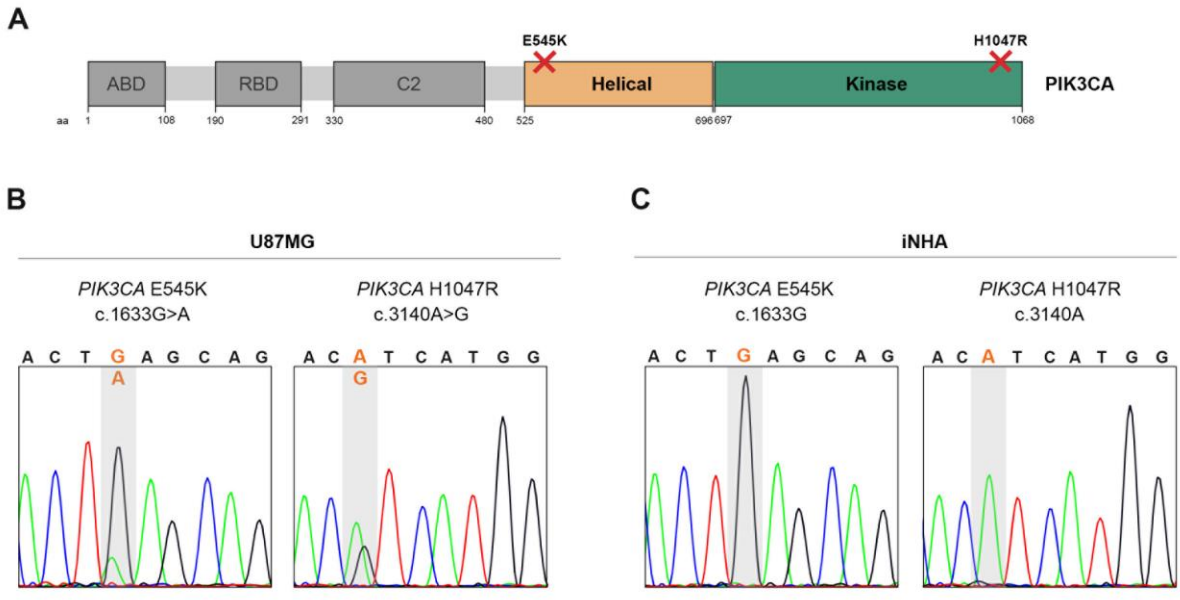

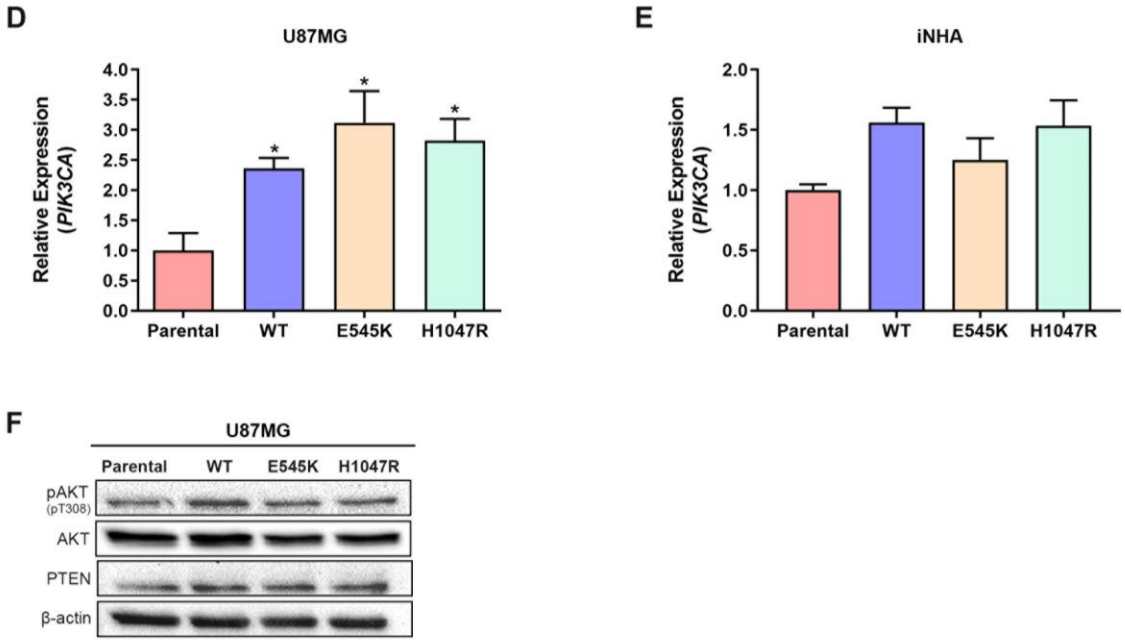

Figure 3.3. Transfection validation of U87MG cells and iNHA. (**A**) Schematic representation of the p110α catalytic subunit of class IA PI3K, also known as PIK3CA, with all five domains represented. The red crosses indicate the most common *PIK3CA* mutations, E545K and H1047R, which also correspond to the mutations that will be introduced in both cell models. ABD, adaptor-binding domain; RBD, Ras-binding domain. (**B**) U87MG transfection validation through cDNA Sanger sequencing. The chromatograms from U87MG cells transfected with the *PIK3CA* E545K plasmid (left) and with the *PIK3CA* H1047R plasmid (right) are represented. The altered nucleotides are highlighted. (**C**) iNHA transfection validation through cDNA Sanger sequencing. The chromatograms from iNHA cells transfected with the *PIK3CA* E545K plasmid (left) and with the *PIK3CA* H1047R plasmid (right) are represented. Alteration of the highlighted nucleotides was not detected. (**D**) RT-qPCR confirming *PIK3CA* overexpression in U87MG cells transfected with *PIK3CA* WT, *PIK3CA* E545K and *PIK3CA* H1047R (mean ± SEM, n=3); **p*<0.05. Unpaired t-test was used to compare between parental cells and each group of transfected cells. (**E**) RT-qPCR comparing *PIK3CA* mRNA levels between parental iNHA and iNHA transfected with *PIK3CA* WT, *PIK3CA* E545K and *PIK3CA* H1047R (mean ± SEM, n=2). Unpaired t-test was used to compare between parental cells and each group of transfected cells. (**F**) Western blot analysis of U87MG transfected cells, with detection of phosphorylated AKT at residue Thr308, total AKT and PTEN as proteins of interest, and β-actin as endogenous control (representative image of all membranes), n=1.

3.4. Impact of E545K and H1047R mutations on U87MG colony formation, cell migration and cell invasion

Since the impact of *PIK3CA* mutations on glioma aggressiveness has been poorly explored, we analyzed in what way the most common *PIK3CA* mutations can alter the behavior of U87MG, a GBM cell line.

Firstly, we evaluated the cells' ability to form colonies (**Figure 3.4 A**). There was no statistically significant difference between the number of colonies formed by U87MG WT, E545K or H1047R cells compared with the parental cell line. However, there seems to be a slight trend for U87MG H1047R cells to form a higher number of colonies compared with parental cells.

We then searched for changes in both cell migration and invasion using transwell assays. Once again, there were no significant differences in the number of migrating and invading U87MG transfected cells when compared with the parental cell line (**Figure 3.4 B-C**).

Lastly, the levels of two enzymes involved in the cancer cell invasion process – matrix metalloproteinase-2 (MMP2) and matrix metalloproteinase-7 (MMP7) – were assessed by Western blot (**Figure 3.4 D**). These enzymes are able to disrupt the extracellular matrix (ECM), facilitating cell invasion[83]. Higher levels of MMP2 were detected in both WT and E545K cells, compared with parental cells, which might indicate that *PIK3CA* overexpression is enough to trigger an increase of MMP2 levels in U87MG cells. However, this increase in MMP2 was not verified in U87MG H1047R cells, which overexpress *PIK3CA* similarly to WT and E545K cells (**Figure 3.4 D**). MMP7 expression, on the other hand, was only elevated in U87MG E545K cells, indicating that *PIK3CA* overexpression is not enough to trigger an increase in MMP7 levels, and that this increase might rely on the presence of the E545K mutation. Either way, these changes in protein expression did not translate to a change in the phenotype of U87MG cells, as there were no differences in the number of invasive cells.

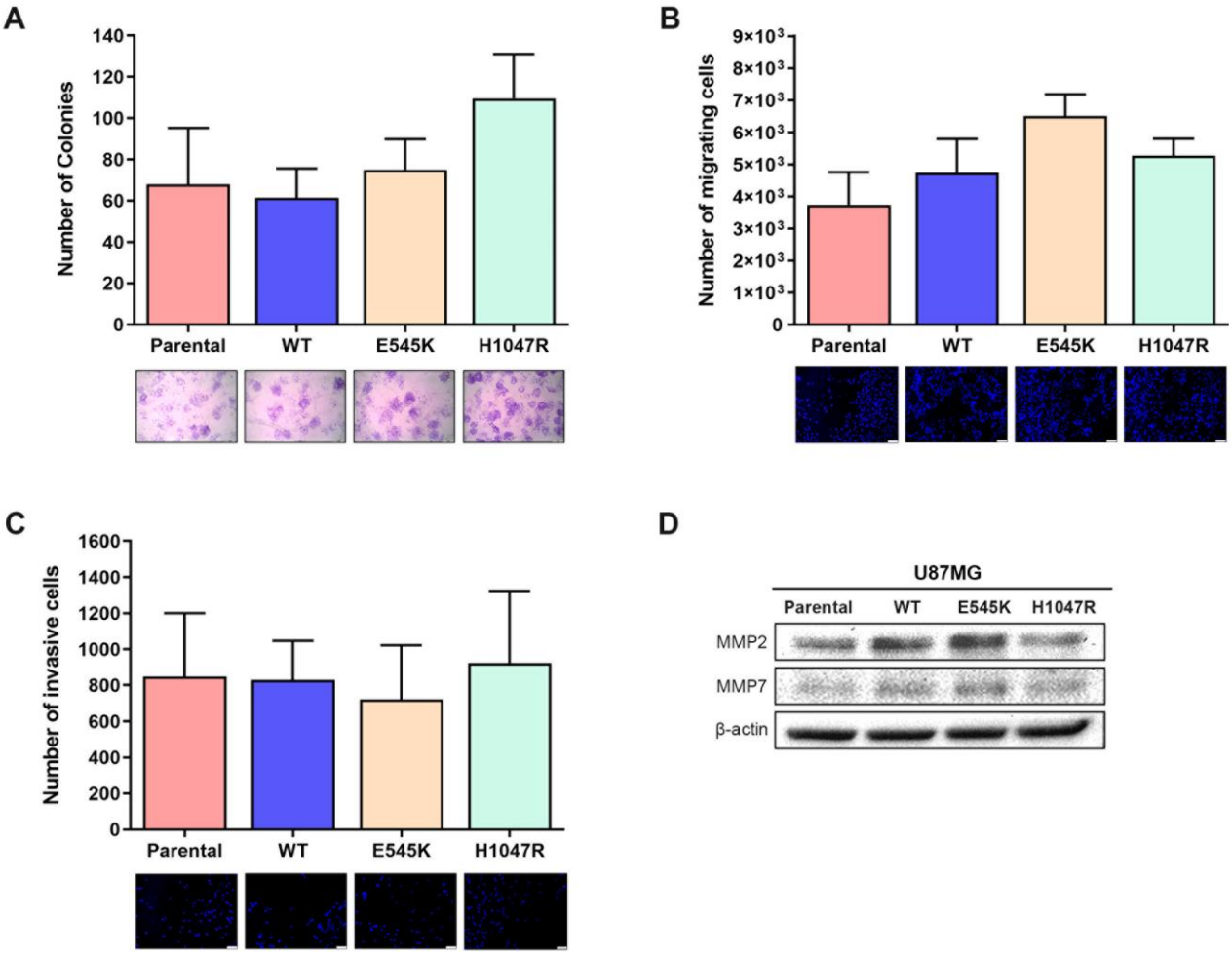

Figure 3.4. Impact of *PIK3CA* mutations E545K and H1047R on the ability of U87MG cells to form colonies, migrate and invade. (**A**) Colony formation of U87MG parental, WT, E545K and H1047R cells, 10 days after seeding. The number of colonies was manually quantified (mean ± SEM, n=4). Representative images are shown. Scale bars = 2 mm (**B**) Migration transwell assay with U87MG parental, WT, E545K and H1047R cells (mean ± SEM, n=5). Representative images are shown. Scale bars = 100 µm. (**C**) Invasion transwell assay with U87MG parental, WT, E545K and H1047R cells (mean ± SEM, n=6). Representative images are shown. Scale bars = 100 µm. (**D**) Western blot analysis of U87MG parental and transfected cells, with detection of MMP2 and MMP7 as proteins of interest, and β-actin as endogenous control (representative image of all membranes), n=1. One-way ANOVA was used to compare between different groups (panels A-C).

3.5. Effect of alpelisib and temozolomide treatments on U87MG cells harboring *PIK3CA* mutations

Even if *PIK3CA* mutations do not seem to have a big impact on the aggressiveness of GBM cells, these alterations might still modulate these cells' response to TMZ treatment, the current chemotherapeutic agent used in GBM[31]. It has been shown that the presence of *PIK3CA* mutations confers resistance to some cancer therapies. For example, the E545K mutation is associated with tumor cell radioresistance, in cervical cancer[67]. Moreover, BYL719, also known as alpelisib, a selective inhibitor of the p110α catalytic subunit of class IA PI3K, is known to increase progression free survival specifically of *PIK3CA* mutant, ER-positive breast cancer patients[70]. Thus, GBM cells harboring *PIK3CA* mutations might be more sensitive to this selective inhibitor, making it a potentially promising therapeutic strategy. In order to validate these hypotheses, we first calculated the half maximal inhibitory concentration (IC_{50}) of both TMZ and alpelisib by assessing the metabolic viability of iNHA and U87MG cells, three and six days after treatment with both compounds (**Figure 3.5 A**). These timepoints allowed us to understand the short- and long-term effects of treatment. BYL719 has a much lower IC_{50} than TMZ, in both cell models, meaning that cells are more sensitive to treatment with this compound. Thus, BYL719 seems to be more toxic to U87MG and iNHA than TMZ. Furthermore, IC_{50} values decrease with longer exposure to each compound, as expected.

Although the IC_{50} was calculated in both cell models, we were only able to do the following assays using U87MG cells, since we could not successfully transfect iNHA. As such, calculating IC_{50} values for TMZ and BYL719 allowed us to choose the two most suitable concentrations to use in the following assays, which could not be overly cytotoxic as to not mask the differences between treatment responses – a concentration close to the IC_{50}, and half of this value. Thus, U87MG cells were treated with 300 µM and 600 µM of TMZ, and 7 µM and 15 µM of BYL719.

The effect of both BYL719 and TMZ treatment on U87MG parental, WT, E545K and H1047R cells was first assessed using a metabolic cell viability assay (**Figure 3.5 B**). TMZ significantly reduced the viability of all cell lines only six days after treatment, with the concentrations chosen being more effective after long exposure. However, there was no statistically significant difference between each cell line's response to treatment. Based on these results, the presence of *PIK3CA* mutations does not make U87MG cells more resistant to TMZ. Surprisingly, BYL719 treatment did not significantly reduce cell viability in any cell line, even though the concentrations used were chosen based on the IC_{50}. Only 15 µM of BYL719 managed to reduce U87MG E545K cell viability three days post treatment, but not at day six. Furthermore, all four cell lines responded to treatment similarly, with no differences detected. Thus, the presence of *PIK3CA* mutations does not enhance GBM cells' sensitivity to the targeted inhibition of PI3Kα.

Cell viability of U87MG transfected cells upon TMZ and alpelisib treatment was assessed once more using the trypan blue assay (**Figure 3.5 C**). Since this is a more sensitive assay, it might detect more subtle differences that the previous assays were unable to. Three days after treatment with TMZ, we could already observe a significant decrease in cell viability – 300 µM only reduced the viabilty of U87MG E545K and H1047R cells, while 600 µM decreased the viability of all four cell lines. Six days

after treatment, TMZ significantly reduced viability of the four cell lines with both concentrations. Once again, no differences were identified between U87MG parental cells and U87MG WT, E545K or H1047R. As for BYL719, at a concentration of 7 µM it was only effective at decreasing the viability of U87MG H1047R cells, three days after treatment. A concentration of 15 µM, however, reduced the viability of all cell lines significantly, after six days of treatment. Interestingly, at this concentration, U87MG E545K cells were more resistant to alpelisib treatment than parental cells, opposite to what was expected. At day six, on the other hand, only 15 µM of BYL719 led to a significant decrease in cell viability, but only of U87MG parental and WT cells. Moreover, we verified that, six days after treatment, U87MG WT cells are more resistant to 7 µM of BYL719 than parental cells, but not to 15 µM of this compound. Overall, both viability assays showed that the presence of *PIK3CA* mutations does not cause GBM cells to become more sensitive or resistant to either compound in a significant way.

The effect of both alpelisib and TMZ treatment on U87MG parental, WT, E545K and H1047R cells was also assessed using Annexin V and PI labeling to calculate total cell death (**Figure 3.5 D**). Preliminary results seem to be in accordance with the previous cell viability results. As we increase the compounds' concentration, there is also an increase in total cell death. Generally, there are no considerable differences between each cell line's response to treatment with either compound. Three days after treatment with 300 µM of TMZ, all three transfected U87MG cells seem to be more resistant than U87MG parental. However, the difference in total cell death is not very pronounced, and this effect is lost with 600 µM, and even with the six-day treatment. Alpelisib had a similar effect after six days of treatment – U87MG WT, E545K and H1047R seem to be more resistant to both 7 µM and 15 µM of this compound, when compared to U87MG parental cells. This effect seems especially pronounced between U87MG parental and U87MG H1047R. It is, however, important to note that these are only preliminary results, and that more independent assays should be performed in order to corroborate them.

Lastly, we assessed the impact of BYL719 and TMZ treatment on the activation of the PI3K/AKT pathway, through Western Blot (**Figure 3.5 E**). TMZ treatment led to a decrease in AKT phosphorylation in all four cell lines, inhibiting this pathway, whilst treatment with selective PI3Kα inhibitor alpelisib did not reduce PI3K/AKT signaling. On the contrary, in U87MG parental cells, treatment with BYL719 at a concentration of 15 µM considerably increased AKT phosphorylation. In U87MG WT cells, this effect was even more pronounced, with both concentrations tested leading to much higher levels of phosphorylated AKT. U87MG H1047R also responded to BYL719 treatment with both concentrations by increasing AKT phosphorylation, although to a lesser extent than U87MG WT cells. The U87MG E545K cell line was the only one that responded in a slightly different manner – treatment with 7 µM BYL719 did, in fact, decrease AKT phosphorylation, but 15 µM BYL719 treatment restored it. Based on these results, it seems that U87MG cells are able to trigger compensatory mechanisms so efficient that they not only revert alpelisib's inhibitory effects, but also potentiate the PI3K/AKT pathway, which could

explain why the presence of *PIK3CA* mutations does not confer more sensitivity to this inhibitor in this cell line, as is the case with other types of cancer.

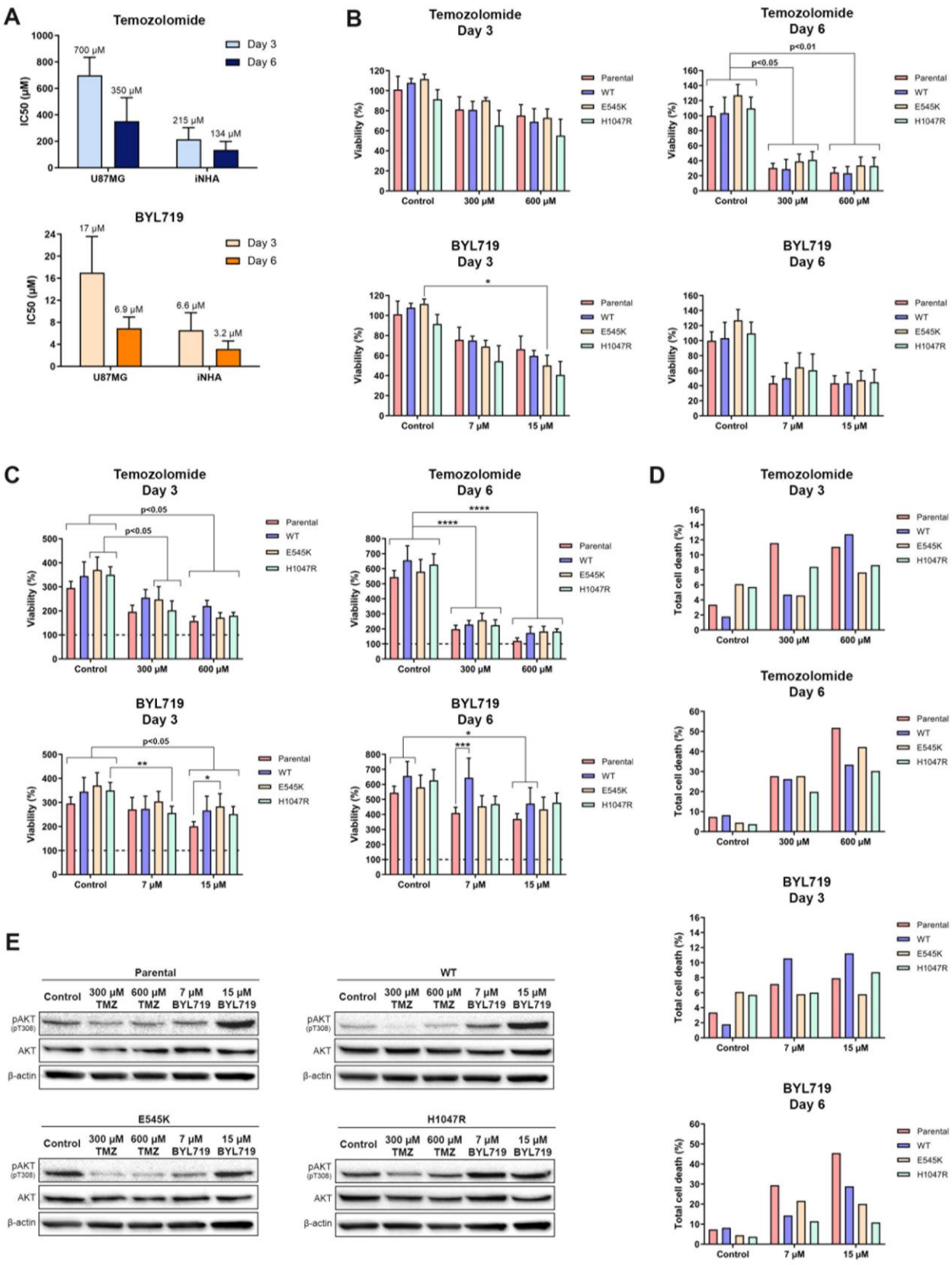

Figure 3.5. Effect of temozolomide and alpelisib (BYL719) on *PIK3CA*-mutant U87MG cells. (**A**) Determination of temozolomide (TMZ) and alpelisib IC_{50} values, three and six days after treatment of U87MG cells and iNHA. Values were obtained using a non-linear regression based on a concentration vs. response variable slope (mean ± SEM, n=3-5). (**B**) U87MG parental, WT, E545K and H1047R cells were treated with vehicle, TMZ (300 µM, 600 µM) or BYL719 (7 µM, 15 µM), and metabolic cell viability was assessed three and six days after treatment, using the CCK8 assay (mean ± SEM, n=3). (**C**) U87MG parental and transfected cells were treated with vehicle, TMZ (300 µM, 600 µM) or BYL719 (7 µM, 15 µM), and cell viability was assessed three and six days after treatment, using the trypan blue assay (mean ± SEM, n=5). (**D**) U87MG parental and transfected cells were treated with vehicle, TMZ (300 µM, 600 µM) or BYL719 (7 µM, 15 µM), and total cell death was assessed three and six days after treatment, using Annexin V/PI labeling (n=1). (**E**) U87MG parental and transfected cells were treated with vehicle, TMZ (300 µM, 600 µM) or BYL719 (7 µM, 15 µM), and total protein was extracted three days after treatment. Western blot analysis was performed, with detection of phosphorylated AKT at residue Thr308 and total AKT as proteins of interest, and β-actin as endogenous control (representative image of all membranes) (n=1). Two-way ANOVA was used to compare between different groups (panels B-C). * $p<0.05$; ** $p<0.01$; *** $p<0.001$; **** $p<0.0001$

4. Discussion

4.1. Reclassification of the IPOLFG glioma cohort based on *IDH2* mutational analysis

The IPOLFG glioma cohort had been previously classified into molecular subgroups based on *IDH1* mutational status and the presence or absence of the 1p/19q codeletion[29]. Concomitantly, it was possible to calculate the percentage of samples harboring *PIK3CA* mutations in each glioma subgroup[65]. However, *IDH2* mutations can also be found in glioma patients, although at a lower frequency, impacting patient stratification and clinical prognosis[28]. More importantly, *IDH* mutations are more frequently present in lower-grade gliomas than in GBM[29,38], and the same was observed in our cohort for *PIK3CA* mutations. Therefore, despite being rare mutations, *IDH2* mutational analysis is somewhat relevant in this context since the presence of these mutations could significantly alter both cohort stratification and *PIK3CA* mutation frequency within each molecular subgroup.

In the present study, we searched for hotspot *IDH2* mutations in the IPOLFG glioma cohort. Only one mutation was found, R172M, in an astrocytoma sample previously classified as *IDH1* wildtype. Hence, only the astrocytoma molecular subgroups suffered alterations, although minimal, and the percentage of *PIK3CA* mutations across subgroups remained unchanged.

In the IPOLFG glioma cohort, the frequency of *IDH1* mutations (29% – 115/394) was much higher than that of *IDH2* mutations (0.3% – 1/394), as described[28,38]. In the TCGA glioma cohort, *IDH1* and *IDH2* mutation frequencies of 51% (408/794) and 2.6% (21/794), respectively, are reported. Similarly, Wang et al. found that 55% (448/811) of gliomas harbored *IDH1* mutations, while only 2.2% (18/881) carried *IDH2* mutations[78]. Consistent with our results, *IDH2* mutations are much rarer than *IDH1* mutations in glioma. However, a higher percentage of *IDH* mutations than what was observed in the IPOLFG cohort has been reported overall. This discrepancy might be due to the differences in sample size, since our cohort is smaller than both TCGA and Wang et al.'s cohorts, and consists mostly of GBM samples, which are less likely to harbor *IDH* mutations when compared to lower-grade gliomas[23].

Despite the IPOLFG cohort not suffering significant changes after this mutational analysis, the search for *IDH2* mutations in addition to *IDH1* mutations remains essential. *IDH* is one of the very few molecular biomarkers proven to be related with better prognosis and clinical outcome in glioma[23]. Thus, misclassification of a tumor harboring an *IDH2* mutation as *IDH*-wildtype can actually impact glioma patient prognosis.

Regarding *PIK3CA* mutations, since their percentage within each molecular subgroup was unchanged after *IDH2* mutational analysis, the subgroups with the highest *PIK3CA* mutation frequency remained *IDH*-mutant and 1p/19q codeleted gliomas and astrocytomas *IDH*-wildtype (10%). Generally, *PIK3CA* mutations are more frequent in lower-grade gliomas when compared with GBM in our cohort, which might indicate a more predominant role for these mutations in LGG. *PIK3CA* mutations are present in only 5% of glioma cases from our cohort; even though it is a small percentage, *PIK3CA* should not be discarded as a potential therapeutic target, especially knowing that there are currently no effective treatments for these patients.

4.2. Immune cell infiltration in *PIK3CA*-mutant gliomas

Previously, using glioma samples from the IPOLFG cohort, our group observed that *PIK3CA* mutations seemed to be maintained during glioma progression regardless of the therapy administered[66]. Thus, we hypothesized that these mutations might contribute to therapy resistance in glioma and explored how the tumor microenvironment could be involved in this process. We evaluated immune cell infiltration estimates of six distinct immune cell subsets, in both LGG and GBM TCGA samples according to *PIK3CA* mutational status, using TIMER. Out of the six subsets analyzed, only CD8+ T cell infiltration was different in *PIK3CA*-mutant samples when compared to *PIK3CA* wildtype. Results suggest that with the presence of *PIK3CA* mutations comes an increase in CD8+ T cell infiltration in LGG.

It is now widely known that cancer cells are constantly interacting with the surrounding environment – TME –, which consists mainly of non-malignant cells (immune cells, fibroblasts, stromal cells), surrounding blood vessels and the extracellular matrix. This crosstalk plays a crucial role in tumor development, therapy response and clinical outcome[84]. CD8+ lymphocytes are amongst the immune cell subsets one can find infiltrating the tumor, responsible for a tumor-specific adaptive immunity response[85]. Therefore, CD8+ T cell infiltration has been linked to better clinical outcomes in breast[85] and colorectal cancer[86]. Historically, it was thought that the brain had immune privilege, meaning that it was immunologically silenced and detached from the rest of the body[87]. While it is true that CNS tumors usually display low numbers of immune infiltrates when compared to other tumors, in recent years it has become clear that immune cells of various subsets and functional lymphatic vessels are present within the CNS[87]. A specific subset of CD8+ lymphocytes designated CD8+ effector T cells can recognize and target glioma cells, and their activation can lead to increased mice survival[88,89]. In contrast, CD8+ regulatory T cells have shown to accumulate in the TME and are associated with tumor-mediated immunosuppression[79]. The TIMER analysis performed does not distinguish between CD8+ T cell subsets and, consequently, we cannot conclude if higher infiltration of these cells in *PIK3CA* mutant tumors supports tumor development or impairs it.

Hence, we next analyzed the correlation between *PIK3CA* expression and various immune cell gene markers in GBM and LGG. No correlation was found for most gene markers, suggesting that *PIK3CA* expression does not heavily modulate the immune microenvironment. Nevertheless, in LGG, a marker for Tregs, *STAT5B*, was positively correlated with *PIK3CA* expression, which could suggest that CD8+ T regulatory cells are in fact the subset of CD8+ lymphocytes that is upregulated in *PIK3CA* mutant LGG samples. Since none of the other Treg markers analyzed displayed significant correlations with *PIK3CA* expression, further research is necessary to confirm these results. Furthermore, Zhong et al. have recently performed a gene expression-based study on immune cell subtypes in glioma and found that CD8+ T cells are associated with worse glioma prognosis[90]. However, this analysis included all gliomas as a single group, with no distinction between molecular subgroups, neither between GBM and LGG[90].

Regarding STAT5B function, it is a signal transducer and activator of transcription and its upregulation was previously found in GBM samples compared with normal brain cortex[91]. This

upregulation was shown to lead to GBM cell growth, cell cycle progression, invasion and migration, making STAT5B an important player in the process of malignant glioma progression and a potential therapeutic target[91]. More importantly, it is known that there is an interaction between STAT5B and the EGFR*vIII* mutated form in the nucleus that promotes therapy resistance, mainly through the activation of the B-cell lymphoma-extra large (*Bcl-XL*) anti apoptotic-marker[92]. This association hints at a possible crosstalk between the PI3K/AKT pathway and the transcriptional factor STAT5B in glioma. Further studies should be conducted to better understand if STAT5B can in fact contribute to the prevalence of *PIK3CA* mutations during glioma progression, and consequently to therapy resistance.

4.3. Impact of *PIK3CA* mutations in glioma aggressiveness

Generally, *PIK3CA* mutations seem to be rarer in glioma than in other cancer types. In breast cancer, about 21%-47% of tumors habor these mutations[93–98], and in colorectal cancer frequencies range from 10% to 38%[58,96,99,100]. In glioma, on the other hand, the overall frequency of *PIK3CA* mutations in the IPOLFG cohort was of 5%. Other studies reported frequencies between 5% to 30%, but always in a specific histological subgroup[57–62]. However, even if *PIK3CA* mutations are rarer in glioma, they still might have therapeutic potential in this small percentage of cases, which becomes quite important as gliomas are considered incurable. Seeing as these mutations are more prevalent in our cohort in lower-grade gliomas, and that TIMER analysis showed associations between *PIK3CA* mutations and the immune microenvironment only in LGG, we can hypothesize that these alterations might be more relevant as therapeutic targets in LGG. Still, it is critical to study, both *in vitro* and *in vivo*, the impact that *PIK3CA* mutations might have on glioma aggressiveness, using both an LGG and a GBM model. Hence, for *in vitro* assays, we chose U87MG cells as a GBM model, and iNHA could mimic a lower-grade glioma, since it is extremely hard to establish an LGG cell line. In order to reach our goal, both models were transfected with plasmids containing: *PIK3CA* WT, *PIK3CA* harboring the E545K mutation and *PIK3CA* harboring the H1047R mutation; these are the two most frequent *PIK3CA* mutations in cancer[51].

Unfortunately, we were only able to successfully transfect one of the models chosen, the U87MG cell line, after increasing both lipofectamine and plasmid DNA quantities added. All three transfected cell lines derived from U87MG – U87MG WT, U87MG E545K and U87MG H1047R – overexpressed the *PIK3CA* gene, which translated in a slight increase in AKT phosphorylation. Additionally, it was possible to detect the respective mutations in U87MG E545K and U87MG H1047R by Sanger sequencing. Thus, it seems that these cells probably need a higher ratio of lipofectamine-plasmid, as well as a higher quantity of plasmid-filled liposomes in order to increase the number of cells that are able to internalize exogenous DNA and go through selection. The same was, however, not verified for iNHA, in which neither increasing plasmid DNA quantity (1-4 µg) nor lipofectamine quantity (20-30 µg) led to the generation of stably transfected cell lines. Moreover, these cells were a lot more sensitive to lipofectamine, and increasing it to 30 µL proved to be cytotoxic. Thus, the optimization of the iNHA transfection protocol is needed.

Due to this setback, we decided to continue research with only one glioma cell model – U87MG. In order to fulfill our goal of studying the impact *PIK3CA* mutations have on glioma aggressiveness, we first assessed the ability of these cells to form colonies. There was a trend for U87MG H1047R cells to form more colonies than the parental cell line, U87MG WT or U87MG E545K. In breast cancer, hotspot mutation H1047R is known to be associated with increased aggressiveness and poorer prognosis than E545K[52,101,102]. In glioma, however, this difference is poorly explored, but some studies point towards a similar effect. McNeill et al. demonstrated that only the H1047R *PIK3CA* mutation promoted colony formation in soft agar, using iNHA as a cell model[55]. *In vivo*, H1047R was shown to modulate the neuronal microenvironment and is, consequently, a driver of gliomagenesis[56]. In our study, the difference between cells harboring the H1047R mutation and parental, WT or E545K was not as pronounced.

On the other hand, when we evaluated the impact of *PIK3CA* mutations on GBM cell migration, there was no statistically significant difference between the migratory capability of U87MG transfected and parental cells. From our knowledge, no other study has explored the impact of *PIK3CA* mutations on the migration or invasion of GBM cells. Nevertheless, recently Xie et al. suggested that, in a *PTEN*-deficient GBM mouse model, cell migration depends mostly on the interaction between p110β and Rac1 rather than the p110α catalytic subunit[103]. This recent study demonstrated that, when the p110α catalytic subunit of PI3K was deleted, there was no change in cell migration ability. Yet, when the p110β subunit was abrogated, there was a drastic decrease in cell migration capability[103]. Thus, if GBM cells rely mostly on p110β for cell migration, the presence of *PIK3CA* mutations that further activate the p110α subunit should not significantly alter the number of migrating cells.

Lastly, when evaluating cell invasion by transwell assays, no differences were detected between the number of invasive U87MG parental, WT, E545K or H1047R cells. However, Western blot analysis showed that MMP2 was being overexpressed in WT and E545K U87MG cells, while MMP7 levels were only increased in U87MG E545K cells. When comparing both assays, it is clear that, in this situation, an increase in matrix metalloproteinase protein expression does not necessarily translate to an increase in cell invasion. Furthermore, it is still unclear if, similarly to GBM cell migration, the catalytic subunit p110β plays a more important role in GBM cell invasion than p110α, which could also explain the lack of differences in the number of invasive cells in the presence or absense of *PIK3CA* mutations.

Overall, *PIK3CA* mutations do not seem to have a significant impact on the aggressiveness of GBM. In addition to different PI3K isoforms possibly having distinct roles in GBM[103], this might also be due to the activation of compensatory mechanisms. The main regulator of the PI3K/AKT pathway is PTEN, which catalyzes the conversion of PIP_3 back to PIP_2[47]. The *PTEN* gene is commonly inactivated in glioma, facilitating the overactivation of the PI3K/AKT pathway[27]. U87MG cells harbor a homozygous *PTEN* mutation, c.209+1G>T, a splice donor variant that likely decreases protein expression[82]. However, as observed in the Western blot analysis from Figure 3.3 F, these cells are still able to produce PTEN, and PTEN levels increase when *PIK3CA* is overexpressed, indicating that this regulatory mechanism is still somewhat active in these cells. Perhaps this feedback loop prevents the PI3K/AKT signaling pathway from being overly activated in the presence of *PIK3CA* mutations, which is consistent

with Western blot results, where the increase in AKT phosphorylation is not profound, and is also accompanied by an increase in PTEN. Thus, the potential impact of *PIK3CA* mutations in GBM aggressiveness is attenuated. This does not seem to be true in other cancer types – using colorectal cancer cells, for example, *PIK3CA* mutations were shown to increase cell growth, migration and invasion *in vitro*[104].

Performing the same assays with another cell model, such as iNHA, would undoubtedly help to interpret the results obtained in U87MG cells. It would be particularly important to see if the results obtained would be similar with both cell models, as iNHA do not harbor any *PTEN* molecular alterations. More importantly, since *PIK3CA* mutations were more prevalent in lower-grade gliomas than in GBM, in the IPOLFG cohort, and there was an association between these alterations and the immune microenvironment in LGG only, the impact these mutations have in iNHA might be completely different from the effect in U87MG cells.

4.4. Pharmacological inhibition of PI3Kα in *PIK3CA*-mutated U87MG cells

Currently, there are no effective glioma therapies, and as such new therapeutic targets are urgently needed, especially considering that these tumors are highly lethal[23]. Even if, based on our results, *PIK3CA* mutations do not exert a significant effect on GBM aggressiveness, these alterations might still show promise as potential therapeutic targets. BYL719, or alpelisib, selectively inhibits PI3Kα, and its effect is generally more pronounced in the presence of *PIK3CA* mutations[53,71–73]. Furthermore, *in vitro* results suggest that mammary epithelial cells harboring hotspot mutations E545K and H1047R are more sensitive to alpelisib treatment, when compared to other mutants and wild-type cells[54]. It has recently been approved as a drug for treatment of patients with advanced ER-positive and *PIK3CA*-mutated breast cancer, leading to an increase in the progression free survival of these patients when combined with fulvestrant administration[70,73]. Thus far, no study has explored PI3Kα inhibition using alpelisib in *PIK3CA*-mutated glioma. Hence, we sought to understand if the presence of *PIK3CA* mutations in a GBM cell model would also enhance its sensitivity to BYL719 treatment, similarly to what is observed in breast cancer. Additionally, we also assessed whether the presence of these mutations modulated GBM cells' response to temozolomide, the most commonly used chemotherapeutic agent in GBM[31].

Firstly, we assessed cell viability upon TMZ and alpelisib treatment by two distinct assays. Results were consistent with both assays – virtually no significant differences in treatment response between U87MG parental, WT, E545K and H1047R cells were detected.

Regarding TMZ, the presence of either E545K or H1047R mutation did not confer resistance to treatment in U87MG cells, as cells transfected with these alterations suffered a reduction in viability similar to that of parental and WT cells. Our group had previously observed that *PIK3CA* mutations were prevalent throughout glioma progression regardless of the therapy administered, which could lead us to believe that these alterations can confer resistance to radio- or chemotherapy. In other cancers, namely breast and colorectal, *PIK3CA* mutations have been associated with therapy resistance, particularly chemotherapy[101,105,106], targeted therapies[94,107–109], and radiotherapy[67]. Our results seem to

suggest, however, that the presence of *PIK3CA* mutations is not enough to confer TMZ resistance to U87MG cells. The fact that these mutations are able to prevail during glioma progression might be due to other mechanisms of therapy resistance, or to the relationship between *PIK3CA* mutations and the immune microenvironment, which we cannot mimic in these assays.

As for alpelisib, the presence of *PIK3CA* mutations did not enhance sensitivity to treatment in this GBM cell model, as cell viability was similar between mutant, WT and parental U87MG cells, for almost all conditions. In the trypan blue viability assay, we observed that, three days after treatment, alpelisib at a concentration of 15 µM led to a significantly smaller decrease in the viability of U87MG cells when compared with the parental. This observation could suggest that the E545K mutations confers U87MG cells with added resistance to alpelisib treatment. However, the same effect was not observed six days after treatment. What we do observe six days after treatment is that 7 µM of alpelisib is more effective at decreasing the viability of parental U87MG cells when compared to WT cells, which could once again suggest that the latter are more resistant to BYL719 treatment. However, this effect was not observed when cells were treated with a higher alpelisib concentration.

In other contexts, such as breast, lung and ovarian cancer, *PIK3CA* mutations usually increase the sensitivity of tumor cells to alpelisib (or other PI3K inhibitors), which makes it such a promising therapeutic strategy for *PIK3CA* mutant tumors[54,74,110,111]. Our results seem to hint that the same might not be true for *PIK3CA* mutant GBM. McNeill et al. encountered a similar response when treating *PIK3CA* mutant iNHA with buparlisib, a PI3K inhibitor that is considered to have activity against all PI3K isoforms, but that in fact demonstrates stronger activity against PI3Kα[55]. In a 2018 *in vitro* study, the authors observed that the presence of *PIK3CA* mutations did not enhance the sensitivy of iNHA to buparlisib treatment[55]. Consistent with the *in vitro* assays, GBM patients with PI3K/AKT pathway activation, including patients with tumors harboring *PIK3CA* mutations, did not benefit from buparlisib treatment[112], indicating that *PIK3CA* mutant GBM cells do not seem to respond to PI3Kα inhibition alone.

We also assessed cell death upon TMZ and BYL719 treatment in U87MG parental, WT, E545K and H1047R cells. Preliminary results seem to be consistent with cell viability results, except six days after treatment with BYL719. Both 7 µM and 15 µM of this compound seem to lead to a higher percentage of total death of U87MG parental cells compared with U87MG WT, E545K or H1047R cells. The H1047R mutation, specifically, seems to be more resistant to cell death upon alpelisib treatment. Even though this resistance is never verified three days after treatment with alpelisib, it could be a late response to treatment with this compound. However, only one independent assay was performed and therefore we cannot take any definitive conclusions.

Lastly, in order to better elucidate the mechanism behind U87MG cells' response to both compounds, we assessed AKT phosphorylation, a downstream effector in the PI3K/AKT pathway, after treatment with BYL719 and TMZ. TMZ treatment reduced PI3K/AKT pathway activation, which is consistent with its function as an alkylating agent that arrests the cell cycle, ultimately triggering tumor cell apoptosis[20]. Importantly, no considerable differences in AKT phosphorylation can be observed between the four cell lines, in accordance with the previous cell viability results. Therefore, the presence

of *PIK3CA* mutations does not change U87MG cells' sensitivity to TMZ treatment.

Surprisingly, treatment with alpelisib did not inhibit AKT phosphorylation; for the most part, this treatment led to an increase in PI3K/AKT pathway activation, which ultimately did not translate to an increase in cell viability or decrease in total cell death. Furthermore, U87MG E545K cells seemed to be the most sensitive to alpelisib exposure, which, once again, is not consistent with cell viability results. It seems that U87MG cells are able to trigger a complex network of compensatory pathways that not only prevent PI3K/AKT pathway inhibition, but can also potentiate its activation. This response is completely distinct from any other type of cancer cell previously tested with alpelisib treatment – it usually results in a significant reduction of phosphorylated AKT, especially in the presence of *PIK3CA* mutations, that can be detected through Western blot[54,113,114]. Perhaps the PI3K/AKT regulator, PTEN, could be involved in these compensatory mechanisms; thus, assessing its levels after alpelisib treatment could be extremely relevant.

Iqbal et al. have previously treated U87MG cells with BYL719 at a concentration of 10 μM, which, opposite to the results presented in this work, led to a decrease in phosphorylated AKT[115]. However, incubation time with BYL719 was of only 90 minutes[115], as opposed to the three-day treatment performed here. A 90-minute period might not be enough for the cells' compensatory mechanisms to kick in, which would explain the disparity in these results. Consequently, it would be interesting to assess the activation of the PI3K/AKT pathway after treatment with alpelisib at various time points.

Xie et al. used both a PTEN-null primary mouse GBM cell line and a PTEN-null patient-derived GBM cell line to demonstrate that treatment with alpelisib is not enough to significantly reduce AKT phosphorylation in GBM[103]. In fact, alpelisib is only able to significantly inhibit the PI3K/AKT pathway if the p110β isoform has been deleted, thus demonstrating that GBM cells are able to use either PI3K catalytic isoform to maintain cell survival[103]. Our results seem to be consistent with the conclusions formed in this study. Maybe the reason there seems to be no significant differences between U87MG parental and WT cells when compared to the *PIK3CA* mutated ones is partly due to a compensation by the p110β isoform upon p110α inhibition. Perhaps this is one of the main differences between GBM and other cancer types, since most solid tumors are dependent on either one PI3K isoform or the other for cell proliferation and survival[116]. Hence, it would also be relevant to assess p110β levels upon BYL719 treatment, in the presence or absence of *PIK3CA* mutations.

Furthermore, metabolism reprogramming by *PIK3CA* mutations might also contribute to these compensatory pathways. Specifically, Hao et al. have shown that, in colorectal cancer cells, *PIK3CA* mutations are able to reprogram glutamine metabolism, culminating in a higher glutamine dependence[117].

Compensatory mechanisms are known to be one of the reasons cells are able to resist to some therapies, including treatment with PI3K inhibitors[118–120]. Studies have reported that, upon treatment with XL147, a PI3K inhibitor, HER2-overexpressing breast cancer cells trigger the upregulation of HER3[119], leading to a compensatory activation of the ERK signaling pathway[120]. As a consequence, PI3K inhibition dampened over time, with phosphorylated AKT levels increasing in a time-dependent manner[119]. Maybe a similar effect would be seen with U87MG cells if we assessed phosphorylated AKT

levels at different time points after alpelisib treatment – alpelisib might in fact reduce PI3K/AKT activation right after treatment, but U87MG cells could trigger compensatory mechanisms that revert this inhibition over time. It could therefore also be relevant to assess the activation of other important pro-survival signaling pathways, such as the mitogen-activated protein kinase (MAPK)/ERK pathway.

Based on the results presented in this work, the best therapeutic strategy to target *PIK3CA*-mutant GBM would probably not go through isoform-specific inhibition. Pan-PI3K inhibitors could be more promising in these cases, although also a lot more challenging, since the PI3K/AKT pathway is essential for the survival and proliferation of all cell types and therefore its complete inhibition is usually associated with higher toxicity and adverse effects[50]. Combining PI3K inhibition with the targeting of other signaling pathways could potentially be the best approach, with some candidates being the ERK/MAPK pathway and also glutamine metabolism[117,119,120].

The use of other glioma cell models is crucial, however, to better interpret these results. A second GBM cell model could corroborate the results obtained, to make sure that they are not cell line specific. Additionally, iNHA could mimick LGG responses to treatment with both compounds, to understand if LGG respond differently than GBM. For example, the compensatory mechanisms triggered in GBM might not be activated in iNHA, and thereby the presence of *PIK3CA* mutations could induce more sensitivity to alpelisib treatment in LGG.

5. Conclusions and Future Perspectives

In the present study, *IDH2* mutational analysis was performed to better characterize the IPOLFG cohort and provide more accurate *PIK3CA* mutation frequencies across all glioma molecular subgroups. Out of 279 samples analyzed, only one harbored a R172M hotspot *IDH2* mutation. Thus, changes implemented to this cohort were minimal, and *PIK3CA* mutation frequencies remained unaltered. *IDH*-mutant and 1p/19q codeleted gliomas and astrocytomas *IDH*-wildtype were the subgroups with the highest *PIK3CA* mutation percentage.

TIMER analysis showed an increase in CD8+ T cell infiltration in *PIK3CA* mutant LGG, which could contribute to the prevalence of *PIK3CA* mutations during glioma progression that had been previously observed in the IPOLFG glioma cohort. Moreover, *PIK3CA* expression was positively correlated with *STAT5B* expression, a marker for T regulatory cells, in LGG samples. In the future, it could be interesting to further investigate these dynamics *in silico*, *in vitro* and *in vivo* in order to understand the importance of the tumor microenvironment in the progression and therapy resistance of *PIK3CA* mutant gliomas. Specifically, it would be relevant to assess what particular CD8+ T cell subset is being upregulated in *PIK3CA* mutant LGG, and the effect this increased infiltration has on tumor progression – if it is a pro-tumoral or anti-tumoral effect. Furthermore, it would be interesting to evaluate the relationship between *PIK3CA* mutations and the immune microenvironment in the distinct glioma molecular subgroups, since we were only able to distinguish between GBM and LGG in the present work.

To explore the impact *PIK3CA* mutations might have on glioma aggressiveness, the U87MG GBM cell line was successfully transfected with three distinct plasmids containing the wildtype *PIK3CA* gene, *PIK3CA* harboring the E545K mutation and *PIK3CA* harboring the H1047R mutation. Both mutations were detected through Sanger sequencing of cDNA. Additionally, *PIK3CA* overexpression was verified in all three cell lines using RT-qPCR, as well as probable PI3K/AKT pathway activation through Western blot. Unfortunately, iNHA transfection was not successful, and all the *in vitro* assays had to be performed with U87MG cells only. To continue this study, the iNHA transfection protocol would have to be optimized. Since these cells were more sensitive to lipofectamine, which could possibly influence the final transfection success rate, a volume of 20 µL or less of lipofectamine would be advised. We could also try increasing and/or decreasing the plasmid concentrations and ajusting the selection antibiotic's concentration. If all of these adjustements proved unsuccessful, we could still try performing different gene editing techniques that do not involve liposomes, such as electroporation, lentiviral transduction, which has a much higher success rate, or even CRISPR-Cas9.

There was a trend for U87MG H1047R cells to form a higher number of colonies than U87MG parental, WT or E545K, which could indicate a slightly more aggressive phenotype in the presence of this specific mutation. On the other hand, the presence of *PIK3CA* mutations did not seem to have an effect on the migratory or invasive capability of U87MG cells. Evidence shows, however, that GBM cells rely mostly on the p110β PI3K catalytic subunit for cell migration, and therefore the presence of *PIK3CA* mutations should not have a great impact on the ability of GBM cells to migrate. It is unclear if the p110β isoform is also predominant in GBM cell invasion. Western blot shows an increase in matrix

metalloproteinases MMP2 and MMP7 in U87MG E545K cells, but this protein overexpression did not translate to a higher number of invasive cells. Our results show that the presence of *PIK3CA* mutations also triggers PTEN overexpression in U87MG cells, which might dampen the overactivation of the PI3K/AKT pathway. As opposed to what happens in other cancer types, such as colorectal and breast cancer, this compensatory mechanism might contribute to the reduced impact of *PIK3CA* mutations in GBM aggressiveness.

Afterward, we intended to understand if the presence of *PIK3CA* mutations in U87MG cells would enhance sensitivity to alpelisib treatment and provide resistance to TMZ treatment. However, when assessing cell viability, the presence of *PIK3CA* mutations does not change U87MG cells' sensitivity to treatment with either alpelisib or temozolomide. Preliminary results for cell death analysis were, for the most part, consistent with the previous cell viability results, except for the indication that cells harboring the H1047R mutation seem to be more resistant to cell death triggered by alpelisib. More independent assays are necessary to confirm these results. Even though our group had previously shown that *PIK3CA* mutations are maintained during glioma progression regardless if therapy had been administered, it seems that the presence of *PIK3CA* mutations is not enough to confer TMZ resistance. Thus, the effect of these mutations on other types of therapy resistance, such as radioresistance, should be further explored, as well as the role the immune microenvironment might play in these processes.

Lastly, we assessed PI3K/AKT pathway activation before and after treatment with both BYL719 and TMZ. While TMZ treatment led to a decrease in AKT phosphorylation, alpelisib surprisingly did not inhibit the PI3K/AKT pathway; instead, it potentiated it, possibly through the activation of compensatory mechanisms involving PTEN, the p110β PI3K isoform, glutamine metabolism or other pro-survival signaling pathways.

In the future, it would be interesting to assess PTEN, p110β and even p110δ levels upon BYL719 treatment, in the presence or absence of *PIK3CA* mutations, using both RT-qPCR and Western blot. We hypothesize that, with an increase in BYL719 concentration, there should also be an increase in p110β, to compensate for p110α inhibition, which would explain the elevated levels of phosphorylated AKT. Maybe p110δ could also play a role in PI3K/AKT regulation in GBM. PTEN levels could potentially be elevated to compensate for the overactivation of the PI3K/AKT pathway. The expression of genes involved in glutamine metabolism before and after BYL719 and TMZ treatment could be relevant, since it could also contribute to this compensatory network, and to TMZ resistance. Furthermore, we could also evaluate the activation of other pro-survival pathways through Western blot, such as the ERK/MAPK pathway.

Most importantly, all assays should be repeated with other glioma cell models. A second GBM cell model, perhaps harboring wildtype *PTEN*, could corroborate the results obtained, while a LGG cell model could give us new insights about the impact *PIK3CA* mutations have in lower-grade gliomas, and how it differs from GBM.

6. References

1. Ruddon, R. W. Characteristics of human cancer. in *Cancer Biology* 3–16 (Oxford University Press, 2007).

2. Yokota, J. Tumor progression and metastasis. *Carcinogenesis* **21**, 497–503 (2000).

3. Bray, F. et al. Global cancer statistics 2018: GLOBOCAN estimates of incidence and mortality worldwide for 36 cancers in 185 countries. *CA. Cancer J. Clin.* **68**, 394–424 (2018).

4. Bishop, J. M. Molecular themes in oncogenesis. *Cell* **64**, 235–248 (1991).

5. Marshall, C. J. Tumor suppressor genes. *Cell* **64**, 313–326 (1991).

6. Hanahan, D. & Weinberg, R. A. The hallmarks of cancer. *Cell* **100**, 57–70 (2000).

7. Hanahan, D. & Weinberg, R. A. Hallmarks of cancer: the next generation. *Cell* **144**, 646–674 (2011).

8. Floor, S. L., Dumont, J. E., Maenhaut, C. & Raspe, E. Hallmarks of cancer: of all cancer cells, all the time? *Trends Mol. Med.* **18**, 509–515 (2012).

9. Munkley, J. & Elliott, D. J. Hallmarks of glycosylation in cancer. *Oncotarget* **7**, 35478–35489 (2016).

10. Fouad, Y. A. & Aanei, C. Revisiting the hallmarks of cancer. *Am. J. Cancer Res.* **7**, 1016–1036 (2017).

11. Furtado, A. D., Panigrahy, A. & Fitz, C. R. Chapter 59 - CNS and spinal tumors. in *Handbook of Clinical Neurology* vol. 136 1139–1158 (Elsevier, 2016).

12. Patel, A. P. et al. Global, regional, and national burden of brain and other CNS cancer, 1990-2016: a systematic analysis for the Global Burden of Disease Study 2016. *Lancet Neurol.* **18**, 376–393 (2019).

13. Louis, D. N. et al. The 2016 World Health Organization classification of tumors of the central nervous system: a summary. *Acta Neuropathol.* **131**, 803–820 (2016).

14. Dang, M. & Phillips, P. C. Pediatric brain tumors. *Contin. Lifelong Learn. Neurol.* **23**, 1727–1757 (2017).

15. Vargo, M. M. Brain tumors and metastases. *Phys. Med. Rehabil. Clin.* **28**, 115–141 (2017).

16. Sanai, N. & Berger, M. S. Glioma extent of resection and its impact on patient outcome. *Neurosurgery* **62**, 753–766 (2008).

17. Englot, D. J., Han, S. J., Berger, M. S., Barbaro, N. M. & Chang, E. F. Extent of surgical resection predicts seizure freedom in low-grade temporal lobe brain tumors. *Neurosurgery* **70**, 921–928 (2012).

18. Correa, D. D. Neurocognitive function in brain tumors. *Curr. Neurol. Neurosci. Rep.* **10**, 232–

239 (2010).

19. Farrell, C. J. & Plotkin, S. R. Genetic causes of brain tumors: neurofibromatosis, tuberous sclerosis, von Hippel-Lindau and other syndromes. *Neurol. Clin.* **25**, 925–946 (2007).

20. Ferris, S. P., Hofmann, J. W., Solomon, D. A. & Perry, A. Characterization of gliomas: from morphology to molecules. *Virchows Arch.* **471**, 257–269 (2017).

21. Davis, M. E. Epidemiology and overview of gliomas. in *Seminars in Oncology Nursing* vol. 34 420–429 (WB Saunders, 2018).

22. Velásquez, C. et al. Molecular and clinical insights into the invasive capacity of glioblastoma cells. *J. Oncol.* **2019**, 1740763 (2019).

23. Reifenberger, G., Wirsching, H. G., Knobbe-Thomsen, C. B. & Weller, M. Advances in the molecular genetics of gliomas — implications for classification and therapy. *Nat. Rev. Clin. Oncol.* **14**, 434–452 (2017).

24. Jäkel, S. & Dimou, L. Glial cells and their function in the adult brain: a journey through the history of their ablation. *Front. Cell. Neurosci.* **11**, 24 (2017).

25. Louis, D. N. et al. The 2007 WHO classification of tumours of the central nervous system. *Acta Neuropathol.* **114**, 97–109 (2007).

26. Kimelberg, H. K. & Nedergaard, M. Functions of astrocytes and their potential as therapeutic targets. *Neurotherapeutics* **7**, 338–353 (2010).

27. van den Bent, M. J. et al. A clinical perspective on the 2016 WHO brain tumor classification and routine molecular diagnostics. *Neuro. Oncol.* **19**, 614–624 (2017).

28. Tateishi, K. & Yamamoto, T. IDH-mutant gliomas. in *Brain and Spinal Tumors - Primary and Secondary* (IntechOpen, 2019).

29. Brito, C. et al. Clinical insights gained by refining the 2016 WHO classification of diffuse gliomas with: EGFR amplification, TERT mutations, PTEN deletion and MGMT methylation. *BMC Cancer* **19**, 968 (2019).

30. Jenkins, R. B. et al. A t(1;19)(q10;p10) mediates the combined deletions of 1p and 19q and predicts a better prognosis of patients with oligodendroglioma. *Cancer Res.* **66**, 9852–9861 (2006).

31. Stupp, R. et al. Radiotherapy plus concomitant and adjuvant temozolomide for glioblastoma. *N. Engl. J. Med.* **352**, 987–996 (2005).

32. Friedman, H. S., Kerby, T. & Calvert, H. Temozolomide and treatment of malignant glioma. *Clin. Cancer Res.* **6**, 2585–2597 (2000).

33. Kawaguchi, T. et al. Impact of gross total resection in patients with WHO grade III glioma harboring the IDH 1/2 mutation without the 1p/19q co-deletion. *J. Neurooncol.* **129**, 505–514

(2016).

34. van den Bent, M. J. & Chang, S. M. Grade II and III oligodendroglioma and astrocytoma. *Neurol. Clin.* **36**, 467–484 (2018).

35. Molinari, E., Curran, O. E. & Grant, R. Clinical importance of molecular markers of adult diffuse glioma. *Pract. Neurol.* **19**, 412–416 (2019).

36. van den Bent, M. J. et al. Adjuvant procarbazine, lomustine, and vincristine chemotherapy in newly diagnosed anaplastic oligodendroglioma: long-term follow-up of EORTC brain tumor group study 26951. *J. Clin. Oncol.* **31**, 344–350 (2013).

37. Kouwenhoven, M. C. M. et al. 1p/19q loss within oligodendroglioma is predictive for response to first line temozolomide but not to salvage treatment. *Eur. J. Cancer* **42**, 2499–2503 (2006).

38. Yan, H. et al. IDH1 and IDH2 mutations in gliomas. *N. Engl. J. Med.* **360**, 765–773 (2009).

39. Xu, W. et al. Oncometabolite 2-hydroxyglutarate is a competitive inhibitor of α-ketoglutarate-dependent dioxygenases. *Cancer Cell* **19**, 17–30 (2011).

40. Curradi, M., Izzo, A., Badaracco, G. & Landsberger, N. Molecular mechanisms of gene silencing mediated by DNA methylation. *Mol. Cell. Biol.* **22**, 3157–3173 (2002).

41. The Cancer Genome Atlas Research Network. Comprehensive, integrative genomic analysis of diffuse lower-grade gliomas. *N. Engl. J. Med.* **372**, 2481–2498 (2015).

42. Weller, M. et al. Molecular classification of diffuse cerebral WHO grade II/III gliomas using genome- and transcriptome-wide profiling improves stratification of prognostically distinct patient groups. *Acta Neuropathol.* **129**, 679–693 (2015).

43. Sasmita, A. O., Wong, Y. P. & Ling, A. P. K. Biomarkers and therapeutic advances in glioblastoma multiforme. *Asia. Pac. J. Clin. Oncol.* **14**, 40–51 (2018).

44. Chen, Y. et al. MGMT promoter methylation and glioblastoma prognosis: a systematic review and meta-analysis. *Arch. Med. Res.* **44**, 281–290 (2013).

45. Napier, C. E. et al. ATRX represses alternative lengthening of telomeres. *Oncotarget* **6**, 16543–16558 (2015).

46. Hobbs, J. et al. Paradoxical relationship between degree of EGFR amplification and outcome in glioblastomas. *Am. J. Surg. Pathol.* **36**, 1186–1193 (2012).

47. Lai, K., Killingsworth, M. C. & Lee, C. S. Gene of the month: PIK3CA. *J. Clin. Pathol.* **68**, 253–257 (2015).

48. Mayer, I. A. & Arteaga, C. L. The PI3K/AKT pathway as a target for cancer treatment. *Annu. Rev. Med.* **67**, 11–28 (2016).

49. Courtney, K. D., Corcoran, R. B. & Engelman, J. A. The PI3K pathway as drug target in human cancer. *J. Clin. Oncol.* **28**, 1075–1083 (2010).

50. Thorpe, L. M., Yuzugullu, H. & Zhao, J. J. PI3K in cancer: divergent roles of isoforms, modes of activation and therapeutic targeting. *Nat. Rev. Cancer* **15**, 7–24 (2015).

51. Vasan, N., Toska, E. & Scaltriti, M. Overview of the relevance of PI3K pathway in HR-positive breast cancer. *Ann. Oncol.* **30**, x3–x11 (2019).

52. Mangone, F. R., Bobrovnitchaia, I. G., Salaorni, S., Manuli, E. & Nagai, M. A. PIK3CA exon 20 mutations are associated with poor prognosis in breast cancer patients. *Clinics* **67**, 1285–1290 (2012).

53. Yang, J. et al. Targeting PI3K in cancer: mechanisms and advances in clinical trials. *Mol. Cancer* **18**, 26 (2019).

54. Vasan, N. et al. Double PIK3CA mutations in cis increase oncogenicity and sensitivity to PI3Kα inhibitors. *Science* **366**, 714–723 (2019).

55. McNeill, R. S. et al. PIK3CA missense mutations promote glioblastoma pathogenesis, but do not enhance targeted PI3K inhibition. *PLoS One* **13**, e0200014 (2018).

56. Yu, K. et al. PIK3CA variants selectively initiate brain hyperactivity during gliomagenesis. *Nature* **578**, 166–171 (2020).

57. Broderick, D. K. et al. Mutations of PIK3CA in anaplastic oligodendrogliomas, high-grade astrocytomas, and medulloblastomas. *Cancer Res.* **64**, 5048–5050 (2004).

58. Samuels, Y. et al. High frequency of mutations of the PIK3CA gene in human cancers. *Science* **304**, 554 (2004).

59. Gallia, G. L. et al. PIK3CA gene mutations in pediatric and adult glioblastoma multiforme. *Mol. Cancer Res.* **4**, 709–714 (2006).

60. Verhaak, R. G. W. et al. Integrated genomic analysis identifies clinically relevant subtypes of glioblastoma characterized by abnormalities in PDGFRA, IDH1, EGFR and NF1. *Cancer Cell* **17**, 98–110 (2010).

61. Lee, J. K. et al. Spatiotemporal genomic architecture informs precision oncology in glioblastoma. *Nat. Genet.* **49**, 594–599 (2017).

62. Tanaka, S. et al. PIK3CA activating mutations are associated with more disseminated disease at presentation and earlier recurrence in glioblastoma. *Acta Neuropathol. Commun.* **7**, 66 (2019).

63. Hartmann, C., Devermann, L., Gehlhaar, C., Holtkamp, N. & von Deimling, A. PIK3CA mutations in oligodendroglial tumours. *Neuropathol. Appl. Neurobiol.* **32**, 209–212 (2006).

64. Pridham, K. J., Varghese, R. T. & Sheng, Z. The role of class IA phosphatidylinositol-4,5-bisphosphate 3-kinase catalytic subunits in glioblastoma. *Front. Oncol.* **7**, 312 (2017).

65. Brito, C. Clinical implications of PIK3CA mutations in gliomas molecular subgroups.

(Universidade Nova de Lisboa, 2018).

66. Brito, C. et al. PIK3CA hotspot mutations in diffuse gliomas: an update on molecular stratification, prognosis, recurrence and aggressiveness. Manuscript in preparation (2020).

67. Jiang, W. et al. Targeting of β-catenin reverses radioresistance of cervical cancer with the PIK3CA-E545K mutation. *Mol. Cancer Ther.* **19**, 337–347 (2020).

68. Potter, C. J., Pedraza, L. G. & Xu, T. Akt regulates growth by directly phosphorylating Tsc2. *Nat. Cell Biol.* **4**, 658–665 (2002).

69. Inoki, K., Li, Y., Zhu, T., Wu, J. & Guan, K. L. TSC2 is phosphorylated and inhibited by Akt and suppresses mTOR signalling. *Nat. Cell Biol.* **4**, 648–657 (2002).

70. De Santis, M. C., Gulluni, F., Campa, C. C., Martini, M. & Hirsch, E. Targeting PI3K signaling in cancer: challenges and advances. *Biochim. Biophys. Acta Rev. Cancer* **1871**, 361–366 (2019).

71. Zhao, H. F. et al. Recent advances in the use of PI3K inhibitors for glioblastoma multiforme: current preclinical and clinical development. *Mol. Cancer* **16**, 100 (2017).

72. Furet, P. et al. Discovery of NVP-BYL719 a potent and selective phosphatidylinositol-3 kinase alpha inhibitor selected for clinical evaluation. *Bioorg. Med. Chem. Lett.* **23**, 3741–3748 (2013).

73. Markham, A. Alpelisib: first global approval. *Drugs* **79**, 1249–1253 (2019).

74. Juric, D. et al. Phosphatidylinositol 3-kinase α–selective inhibition with alpelisib (BYL719) in PIK3CA-altered solid tumors: results from the first-in-human study. *J. Clin. Oncol.* **36**, 1291–1299 (2018).

75. Massacesi, C. et al. PI3K inhibitors as new cancer therapeutics: implications for clinical trial design. *Onco. Targets. Ther.* **9**, 203–210 (2016).

76. Li, T. et al. TIMER: a web server for comprehensive analysis of tumor-infiltrating immune cells. *Cancer Res.* **77**, e108–e110 (2017).

77. Livak, K. J. & Schmittgen, T. D. Analysis of relative gene expression data using real-time quantitative PCR and the 2-ΔΔCT method. *methods* **25**, 402–408 (2001).

78. Wang, H. Y. et al. The comparison of clinical and biological characteristics between IDH1 and IDH2 mutations in gliomas. *J. Exp. Clin. Cancer Res.* **35**, 86 (2016).

79. Wang, R. F. CD8+ regulatory T cells, their suppressive mechanisms, and regulation in cancer. *Hum. Immunol.* **69**, 811–814 (2008).

80. Barker, H. E., Paget, J. T. E., Khan, A. A. & Harrington, K. J. The tumour microenvironment after radiotherapy: mechanisms of resistance and recurrence. *Nat. Rev. Cancer* **15**, 409–425 (2015).

81. Senthebane, D. A. et al. The role of tumor microenvironment in chemoresistance: to survive, keep your enemies closer. *Int. J. Mol. Sci.* **18**, 1586 (2017).

82. Clark, M. J. et al. U87MG decoded: the genomic sequence of a cytogenetically aberrant human cancer cell line. *PLoS Genet.* **6**, e1000832 (2010).

83. Gonzalez-Avila, G. et al. Matrix metalloproteinases participation in the metastatic process and their diagnostic and therapeutic applications in cancer. *Crit. Rev. Oncol. Hematol.* **137**, 57–83 (2019).

84. Hui, L. & Chen, Y. Tumor microenvironment: sanctuary of the devil. *Cancer Lett.* **368**, 7–13 (2015).

85. Mahmoud, S. M. A. et al. Tumor-infiltrating CD8+ lymphocytes predict clinical outcome in breast cancer. *J. Clin. Oncol.* **29**, 1949–1955 (2011).

86. Galon, J. et al. Type, density, and location of immune cells within human colorectal tumors predict clinical outcome. *Science* **313**, 1960–1964 (2006).

87. Sampson, J. H., Gunn, M. D., Fecci, P. E. & Ashley, D. M. Brain immunology and immunotherapy in brain tumours. *Nat. Rev. Cancer* **20**, 12–25 (2020).

88. Kleijn, A. et al. The sequence of Delta24-RGD and TMZ administration in malignant glioma affects the role of CD8+T cell anti-tumor activity. *Mol. Ther.* **5**, 11–19 (2017).

89. Zeng, J. et al. Anti-PD-1 blockade and stereotactic radiation produce long-term survival in mice with intracranial gliomas. *Int. J. Radiat. Oncol. Biol. Phys.* **86**, 343–349 (2013).

90. Zhong, Q. Y. et al. A gene expression-based study on immune cell subtypes and glioma prognosis. *BMC Cancer* **19**, 1116 (2019).

91. Liang, Q. C. et al. Inhibition of transcription factor STAT5b suppresses proliferation, induces G1 cell cycle arrest and reduces tumor cell invasion in human glioblastoma multiforme cells. *Cancer Lett.* **273**, 164–171 (2009).

92. Latha, K. et al. Nuclear EGFRvIII-STAT5b complex contributes to glioblastoma cell survival by direct activation of the Bcl-XL promoter. *Int. J. cancer* **132**, 509–520 (2013).

93. Stemke-Hale, K. et al. An integrative genomic and proteomic analysis of PIK3CA, PTEN, and AKT mutations in breast cancer. *Cancer Res.* **68**, 6084–6091 (2008).

94. Loibl, S. et al. PIK3CA mutations are associated with lower rates of pathologic complete response to anti-human epidermal growth factor receptor 2 (HER2) therapy in primary HER2-overexpressing breast cancer. *J. Clin. Oncol.* **32**, 3212–3220 (2014).

95. Yuan, W. et al. S100a4 upregulation in Pik3caH1047R;Trp53R270H;MMTV-Cre-driven mammary tumors promotes metastasis. *Breast Cancer Res.* **21**, 152 (2019).

96. Millis, S. Z. et al. Phosphatidylinositol 3-kinase pathway genomic alterations in 60,991 diverse solid tumors informs targeted therapy opportunities. *Cancer* **125**, 1185–1199 (2019).

97. The Cancer Genome Atlas Network. Comprehensive molecular portraits of human breast

tumours. *Nature* **490**, 61–70 (2012).

98. Deng, L. et al. Prevalence and prognostic role of PIK3CA/AKT1 mutations in Chinese breast cancer patients. *Cancer Res. Treat.* **51**, 128–140 (2019).

99. Stec, R. et al. Mutation of the PIK3CA gene as a prognostic factor in patients with colorectal cancer. *Oncol. Lett.* **10**, 1423–1429 (2015).

100. Chiu, J. W. et al. Molecular profiling of patients with advanced colorectal cancer: Princess Margaret Cancer Centre experience. *Clin. Colorectal Cancer* **17**, 73–79 (2018).

101. Guo, S. et al. PIK3CA H1047R mutation associated with a lower pathological complete response rate in triple-negative breast cancer patients treated with anthracycline-taxane–based neoadjuvant chemotherapy. *Cancer Res. Treat.* **52**, 689–696 (2020).

102. Meyer, D. S. et al. Expression of PIK3CA mutant E545K in the mammary gland induces heterogeneous tumors but is less potent than mutant H1047R. *Oncogenesis* **2**, e74 (2013).

103. Xie, S. et al. Divergent roles of PI3K isoforms in PTEN-deficient glioblastomas. *Cell Rep.* **32**, 108196 (2020).

104. Samuels, Y. et al. Mutant PIK3CA promotes cell growth and invasion of human cancer cells. *Cancer Cell* **7**, 561–573 (2005).

105. Mosele, F. et al. Outcome and molecular landscape of patients with PIK3CA-mutated metastatic breast cancer. *Ann. Oncol.* **31**, 377–386 (2020).

106. Wang, Q. et al. PIK3CA mutations confer resistance to first-line chemotherapy in colorectal cancer. *Cell Death Dis.* **9**, 739 (2018).

107. Cizkova, M. et al. Outcome impact of PIK3CA mutations in HER2-positive breast cancer patients treated with trastuzumab. *Br. J. Cancer* **108**, 1807–1809 (2013).

108. Berns, K. et al. A functional genetic approach identifies the PI3K pathway as a major determinant of trastuzumab resistance in breast cancer. *Cancer Cell* **12**, 395–402 (2007).

109. Xu, J. M. et al. PIK3CA mutations contribute to acquired cetuximab resistance in patients with metastatic colorectal cancer. *Clin. Cancer Res.* **23**, 4602–4616 (2017).

110. Janku, F. et al. PI3K/AKT/mTOR inhibitors in patients with breast and gynecologic malignancies harboring PIK3CA mutations. *J. Clin. Oncol.* **30**, 777–782 (2012).

111. Shi, R. et al. Targeting the CDK4/6-Rb pathway enhances response to PI3K inhibition in PIK3CA-mutant lung squamous cell carcinoma. *Clin. Cancer Res.* **24**, 5990–6000 (2018).

112. Wen, P. Y. et al. Phase II trial of the phosphatidyinositol (PI3K) inhibitor buparlisib (BKM120) in recurrent glioblastoma conducted by the Ivy Foundation Early Phase Clinical Trials Consortium. *Neuro. Oncol.* **16**, iii47 (2014).

113. Nölting, S. et al. The selective PI3Kα inhibitor BYL719 as a novel therapeutic option for

neuroendocrine tumors: results from multiple cell line models. *PLoS One* **12**, e0182852 (2017).

114. Zhang, C., Xu, B. & Liu, P. Addition of the p110α inhibitor BYL719 overcomes targeted therapy resistance in cells from Her2-positive-PTEN-loss breast cancer. *Tumor Biol.* **37**, 14831–14839 (2016).

115. Iqbal, A. et al. Targeting of glioblastoma cell lines and glioma stem cells by combined PIM kinase and PI3K-p110α inhibition. *Oncotarget* **7**, 33192–33201 (2016).

116. Utermark, T. et al. The phosphatidylinositol 3-kinase (PI3K) isoform dependence of tumor formation is determined by the genetic mode of PI3K pathway activation rather than by tissue type. *J. Virol.* **88**, 10673–10679 (2014).

117. Hao, Y. et al. Oncogenic PIK3CA mutations reprogram glutamine metabolism in colorectal cancer. *Nat. Commun.* **7**, 11971 (2016).

118. Tomar, V. S., Patil, V. & Somasundaram, K. Temozolomide induces activation of Wnt/β-catenin signaling in glioma cells via PI3K/Akt pathway: implications in glioma therapy. *Cell Biol. Toxicol.* **36**, 273–278 (2020).

119. Chakrabarty, A., Sánchez, V., Kuba, M. G., Rinehart, C. & Arteaga, C. L. Feedback upregulation of HER3 (ErbB3) expression and activity attenuates antitumor effect of PI3K inhibitors. *Proc. Natl. Acad. Sci.* **109**, 2718–2723 (2012).

120. Serra, V. et al. PI3K inhibition results in enhanced HER signaling and acquired ERK dependency in HER2-overexpressing breast cancer. *Oncogene* **30**, 2547–2557 (2011).